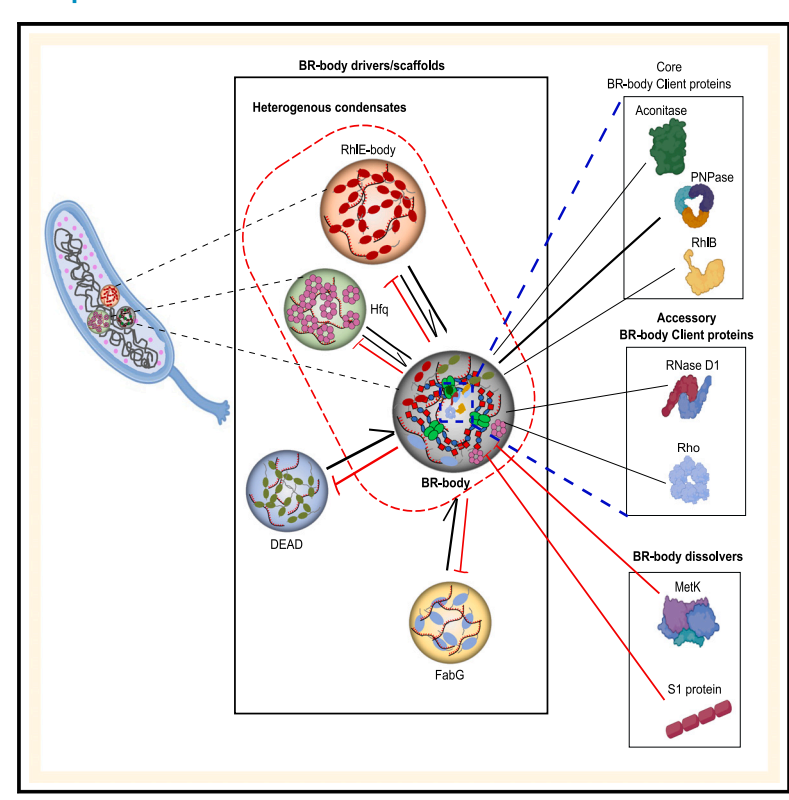
The BR-body proteome contains a complex network of protein-protein and protein-RNA interactions

Graphical abstract



Authors

Vidhyadhar Nandana, Imalka W. Rathnayaka-Mudiyanselage, Nisansala S. Muthunayake, ..., Matthew M. Champion, W. Seth Childers, Jared M. Schrader

Correspondence

schrader@wayne.edu

In brief

Nandana et al. present liquid chromatography-mass spectrometry proteomics data of bacterial RNP bodies, revealing that they contain >100 proteins including the RNA degradosome.

Through the complex network of protein-protein and protein-RNA interactions, this proteome has diverse regulatory interactions with the core scaffold RNase E that impact BR-body assembly and function.

Highlights

- Bacterial RNP body (BR-body) proteomics identifies 111 proteins enriched in BR-bodies
- BR-bodies associate with an interconnected network of RNP condensates
- BR-body condensation is modulated by its interaction network
- RNA is required for rapid BR-body condensation







Article

The BR-body proteome contains a complex network of protein-protein and protein-RNA interactions

Vidhyadhar Nandana, ^{1,10} Imalka W. Rathnayaka-Mudiyanselage, ^{1,2,10} Nisansala S. Muthunayake, ^{1,9} Ali Hatami, ³ C. Bruce Mousseau, ⁴ Luis A. Ortiz-Rodríguez, ⁵ Jamuna Vaishnav, ^{3,8} Michael Collins, ⁶ Alisa Gega, ^{1,7} Kaveendya S. Mallikaarachchi, ¹ Hadi Yassine, ¹ Aishwarya Ghosh, ¹ Julie S. Biteen, ⁵ Yingxi Zhu, ³ Matthew M. Champion, ⁴ W. Seth Childers, ⁶ and Jared M. Schrader ^{1,11,*}

SUMMARY

Bacterial ribonucleoprotein bodies (BR-bodies) are non-membrane-bound structures that facilitate mRNA decay by concentrating mRNA substrates with RNase E and the associated RNA degradosome machinery. However, the full complement of proteins enriched in BR-bodies has not been defined. Here, we define the protein components of BR-bodies through enrichment of the bodies followed by mass spectrometry-based proteomic analysis. We find 111 BR-body-enriched proteins showing that BR-bodies are more complex than previously assumed. We identify five BR-body-enriched proteins that undergo RNA-dependent phase separation *in vitro* with a complex network of condensate mixing. We observe that some RNP condensates coassemble with preferred directionality, suggesting that RNA may be trafficked through RNP condensates in an ordered manner to facilitate mRNA processing/decay, and that some BR-body-associated proteins have the capacity to dissolve the condensate. Altogether, these results suggest that a complex network of protein-protein and protein-RNA interactions controls BR-body phase separation and RNA processing.

INTRODUCTION

Biomolecular condensates have been shown to be an important mode of subcellular organization in eukaryotes and bacteria. 1-3 As bacteria often lack membrane-bound organelles, biomolecular condensates may provide a generalized strategy for their subcellular organization. Indeed, many bacterial biomolecular condensates have been recently identified in various species, including bacterial ribonucleoprotein bodies (BR-bodies), signaling condensates, DNA replication condensates, RNApol condensates, Hfq condensates, Rubisco condensates, etc. 4-10 Biomolecular condensates typically assemble through the physical process of phase separation, which involves association of macromolecular scaffolds and segregation of other cellular components, ultimately leading to distinct non-membrane-bound structures. 11 Recent analyses of condensate physical properties appear to be consistent with a model of percolation-coupled phase separation, which includes both associative interactions as well as segregative, ¹² leading to phase separation. ¹³ Macromolecules that have the capacity to phase separate are referred to as scaffolds, which generally provide a platform for the multivalent interactions that lead to phase separation. Molecules that are recruited to condensates but cannot phase separate themselves are called clients. 14 A condensate's composition of scaffolds and clients determines its biochemical and cellular function. Importantly, molecules inside of condensates often show diffusive dynamics, suggesting that biomolecular condensates facilitate the biochemical processes within them. 15,16 Several models have been proposed for how condensates might accelerate enzyme-catalyzed processes, including increasing reaction rates by raising the local concentration of substrates and enzymes, increasing reaction specificity by the selective recruitment of certain substrates and avoidance of others, and increasing reaction completion by preventing the release of pathway intermediates. 17-19 Conversely, biomolecular condensates have also been proposed to sequester substrate



¹Department of Biological Sciences, Wayne State University, Detroit, MI 48202, USA

²Department of Chemistry, Wayne State University, Detroit, MI 48202, USA

³Department of Chemical Engineering and Materials Science, Wayne State University, Detroit, MI 48202, USA

⁴Department of Chemistry, University of Notre Dame, Notre Dame, IN 46556, USA

⁵Department of Chemistry, University of Michigan, Ann Arbor, MI 48109, USA

⁶Department of Chemistry, University of Pittsburgh, Pittsburgh, PA 15260, USA

⁷Present address: University of Toledo Medical School, Toledo, OH 43606, USA

⁸Present address: University of Massachusetts, Amherst, MA 01003, USA

⁹Present address: Department of Biochemistry, Faculty of Medicine, Wayamba University of Sri Lanka, Kuliyapitiya, North Western Province 60200, Sri Lanka

¹⁰These authors contributed equally

¹¹Lead contact

^{*}Correspondence: schrader@wayne.edu https://doi.org/10.1016/j.celrep.2023.113229





molecules from their enzymes, leading to a reduction in reaction rates. 20,21 Therefore, it is important to identify the molecular components of the condensate to determine the biochemical consequences of biomolecular condensate organization.

Despite advances in biomolecular condensate biochemistry, many in vitro studies have focused on purified scaffolds, and often lack the full suite of molecules identified to interact in vivo. This is potentially problematic, as proteomic/transcriptomic investigations in eukaryotes have revealed that biomolecular condensates are enriched in hundreds of different molecules that may alter their biochemical or cellular functions. For example, P-bodies have been found to contain >125 proteins and >6,000 RNA transcripts,²² and appear to concentrate mRNA decay enzymes (including decapping enzymes, LSM proteins, Xrn1 nuclease, deadenylases, etc.) together with decapped and translationally repressed mRNAs. Stress granules have been found to contain >300 proteins and >1,800 RNA transcripts, 23-25 including a partially overlapping set of components with P-bodies, 22,26 yet the differences in composition and slower dynamics²⁷ suggests that these structures likely have distinct functions. Through careful quantitative measurements, the core set of P-body proteins has recently been reconstituted in vitro, with similar dynamic properties.²⁸ In bacteria, BR-bodies were found to be enriched in long, poorly translated mRNAs and sRNAs, a class of translational repressors, together with RNA degradosome proteins. 4,29 Therefore, it was assumed that BRbodies have a small set of protein clients that could be amendable to in vitro reconstitution²⁷; however, the full complement of proteins in BR-bodies has not been identified.

To define the proteome of Caulobacter crescentus BR-bodies, we performed enrichment by differential centrifugation³⁰ followed by quantitative liquid chromatography-tandem mass spectrometry (LC-MS-MS). Like eukaryotic condensates, we identified >100 proteins that were enriched in BR-bodies. Enriched proteins tended to localize into foci in vivo and enter RNase E condensates in vitro, suggesting that many are likely direct clients of RNase E, the main BR-body scaffold. While most enriched proteins do not assemble into biomolecular condensates in vitro, we identified five BR-body-associated proteins that can undergo phase separation without RNase E, suggesting that they form distinct ribonucleoprotein (RNP) condensates in the cells that interact with RNase E. By assaying the pairwise ability of each scaffold protein to mix with the others, we observed that some pairs of scaffolds have strong associations, and that certain pairs show preferred directional recruitment, which likely impacts RNP assembly order, leading to heterogeneous RNP condensates in vivo. We also identified two proteins that can dissolve BR-bodies both in vivo and in vitro, suggesting that they negatively regulate BR-body assembly. Despite the identification of many BR-body-associated proteins, the RNA degradosome proteins are the only proteins identified that stoichiometrically bind to RNase E31 and that are uniformly colocalized with RNase E foci in vivo, suggesting that a minimal BRbody can be reconstituted. Minimal BR-body phase separation was kinetically stimulated by RNA and showed similar RNase E FRAP dynamics to RNase E-RNA droplets. Overall, this suggests that BR-bodies have similar complex interaction networks to eukaryotic RNP condensates, and the reconstitution of the "core"

minimal BR-body components provides an exciting framework to begin assessing biochemical functions and how they might be altered by the addition of BR-body-associated proteins.

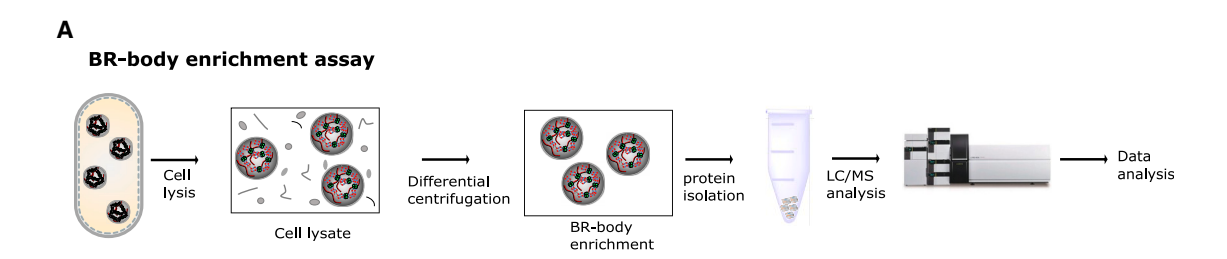
RESULTS

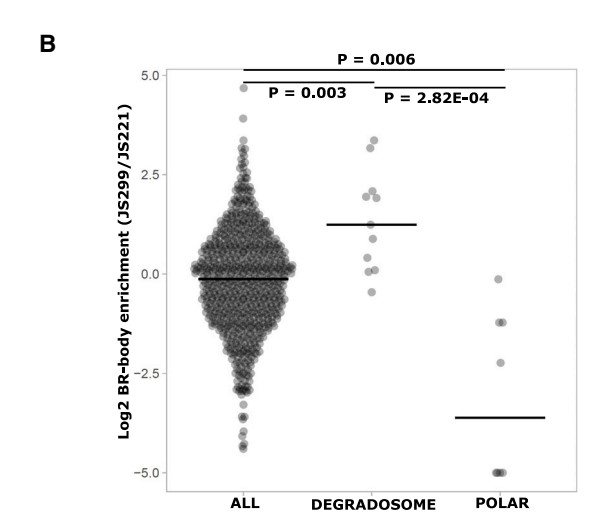
Characterization of the BR-body proteome by LC-MS proteomics

To define the Caulobacter crescentus (Caulobacter) BR-bodyassociated proteome, BR-body enrichment was performed as in Muthunayake et al.30 and subjected to bottom-up proteomics preparation and analysis (Figure 1A; Table S1). BR-body-enriched samples were compared with a mock-treated lysate of a mutant that is unable to assemble BR-bodies due to IDR deletion of RNase E. 30 100 µg protein was prepared in triplicate for either condition and converted into peptides via enzymatic digestion using S-Traps.32 Each sample was analyzed by LC-MS in technical triplicate. Peptide-spectral matching, protein inference, and label-free quantification (LFQ) were performed using FlashLFQ in MetaMorpheus.33 Data were filtered to a false discovery rate of 1.0% and exported as text for analysis. Using these parameters, a total of 1079 proteins were identified in both samples, and the ratio of signal in the BR-body-enriched sample (JS299) over the negative control (JS221) was plotted (Figure 1B). One hundred and eleven proteins were identified to be enriched in BR-bodies. These enriched proteins had a Log2 BR-body enrichment value of >1 (>2-fold enrichment) with a >95% confidence interval (resulting p values subject to Benjamini-Hochberg correction) or were identified in all three biological replicates in BR-body-enriched samples but were not detected in the negative control. These enriched proteins were predominantly cytoplasmic, while proteins derived from other cellular compartments were depleted, suggesting that reasonable enrichment of BR-bodies occurred in the sample. In addition, we observed significantly higher scores for known RNase E-associated proteins, while proteins that interact with polar biomolecular condensates were depleted (Figure 1B), suggesting that the enrichment was not contaminated with all cellular condensates. GO-term analysis of BR-body-enriched proteins revealed RNA binding, ATP binding, GTPase activity, and RNA degradation functionalities (Figure 1B).

To validate whether BR-body-enriched proteins localize into BR-bodies in vivo, we examined the ability of enriched proteins to localize into foci in vivo, the foci's dependence on RNase E, and the proteins' colocalization with BR-bodies. To comprise the set of BR-body-enriched proteins, we chose proteins that are part of the Caulobacter RNA degradosome, 31,34 proteins that associate with RNase E in the cold, 35 and proteins that are known to have a role in RNA processes. We selected proteins with no known role in RNA processes (DnaK and FabG) as a negative control. In addition, we also chose a set of proteins that were not enriched in BR-bodies, but function in RNA decay. We expressed each protein fused with YFP from the vanillate locus (Figure S1) and measured the average foci/cell (Figure 2A). Importantly, even when expressed highly in Caulobacter, YFP is not sufficient to form foci.³⁸ Interestingly, 7/12 proteins from the BR-body-enriched set assembled into foci in vivo, while only 2/10 proteins showed foci (RNase HI and MetK) from







Enriched	Number of proteins	p-value
Cytoplasm	32	9.40E-11
Depleted	•	·
Membrane	160	3.90E-23
Transmembrane	126	2.30E-12
Cell inner membrane	33	3.00E-12
Transmembrane helix	121	3.80E-11
Cell membrane	40	4.30E-11
Cell outer membrane	7	1.30E-03
Cell wall	5	6.40E-02

Enriched N	Number of proteins p-value		
RNA Binding	14	9.00E-07	
ATP Binding	19	8.80E-03	
RNA Degradation	5	9.90E-03	
GTPase Activity	5	3.80E-03	

Figure 1. BR-body enrichment proteomics identifies BR-body-associated proteins

(A) Caulobacter crescentus BR-body enrichment was performed, followed by LC-MS/MS proteomics to identify BR-body-associated proteins. JS299 (an RNase E active site mutant) was used to isolate BR-bodies, and JS221 (an RNase E mutant that cannot form BR-bodies) was used as a negative control. The average enrichment is calculated from three biological replicates.

(B) BR-body enrichment analysis from the LC-MS/MS proteomics data. The RNA degradosome proteins were identified by pull-down. 31,34,35 Polar proteins were identified as interactors with PopZ³⁶ or polar condensates with interactions with PopZ, PodJ, or SpmX. Polar proteins measured in the negative control but undetected in the BR-body-enriched samples were plotted at <-5. t tests with uneven variance were used for statistical comparison. GO-term enrichment for localization and protein function were performed using NCBI DAVID.³⁷

depleted proteins. Of the 5/12 proteins that were enriched but did not form foci, it is possible that the C-terminal YFP tag interfered with their ability to form foci, as SmpB, which was found to form foci by immunofluorescence³⁹ but not by YFP-fusion.

To test whether the observed foci were BR-bodies, we examined the colocalization of foci with either the core BR-body scaffold RNase E or core degradosome protein Aconitase.4 To examine colocalization, we drew a line across the foci of each protein, and then correlated the intensity between this channel and that of the BR-body marker (Figure 2B). As a negative control, we included PopZ, a protein that can form a polar biomolecular condensate involved in cell signaling.36 We could not visualize PNPase-YFP together with RNase E-mCherry or Aconitase-mCherry as we noticed very slow growth. We found that, for the core degradosome proteins Aconitase and RhIB,³¹ foci were uniformly colocalized with RNase E in all cases (average correlation = 0.94 Aconitase, 0.92 RhlB), while RNase E foci did not correlate with PopZ foci (average correlation = 4.8×10^{-3}). We found that RNase D1, RhIE, Rho, and Hfq showed significant but heterogeneous colocalization with BRbodies (average correlation = 0.32 RNase D1, 0.39 RhIE, 0.72 Rho, 0.52 Hfq), while BR-body-depleted proteins RNase H1

and MetK showed no correlation (average correlation = 3.1 \times 10^{-2} MetK, 6.1 × 10^{-2} RNase H1), like the PopZ control, suggesting they are indeed not enriched in BR-bodies. Interestingly, RNase D1 was found to be RNase E associated³⁴ but was depleted in the BR-body proteomics data, while RNase D2 was found to be highly enriched in BR-bodies, suggesting that they may be interchangeable. We observed that RNase D1-YFP appeared to be localized to the inner membrane, suggesting that perhaps it was lost upon the initial membrane pelleting step of the BR-body enrichment procedure. Consistent with this hypothesis, we observed significant colocalization between RNase D1-YFP and RNase E-mCherry in live cells (Figure 2B). We did not observe foci of RNase D2-YFP (Figures 2A and S1), suggesting that either it is not-enriched in BR-bodies, or that the YFP tag disrupts localization. The heterogeneity of RNase D1, RhIE, and Hfg suggests that they are present in a subset of BR-bodies.

Identification of BR-body-associated scaffolds that condense without RNase E

Since RNase E is necessary and sufficient to form BR-bodies.4 we tested whether RNase E was required for BR-body-enriched proteins to form foci (Figure 2C). Because RNase E is essential,



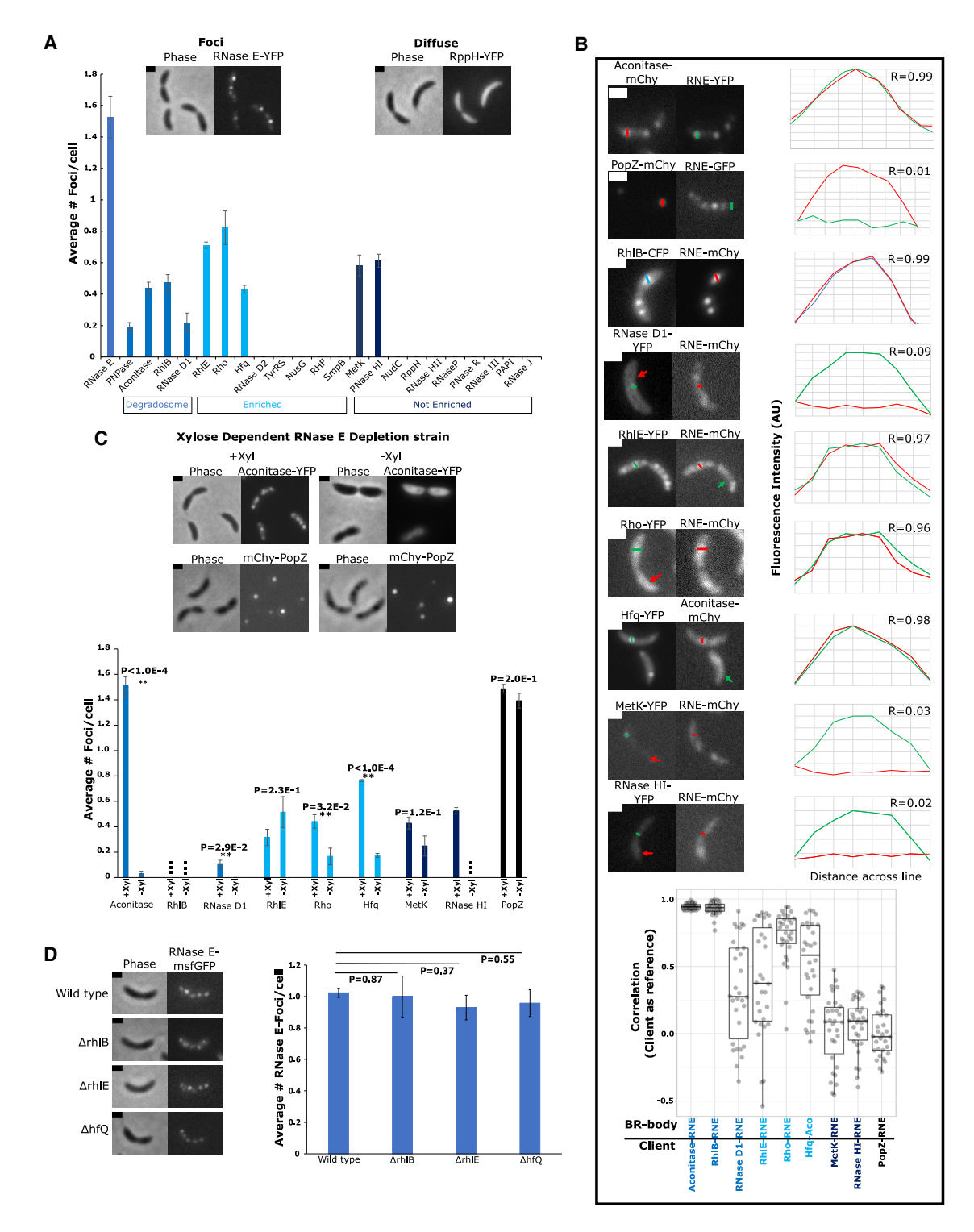


Figure 2. RNase E is required for the foci formation and BR-body colocalization of most BR-body-associated proteins

(A) The localization pattern of foci-forming YFP-fusions. In vivo, YFP-fusion strains were analyzed at mid-exponential phase of growth (OD 0.3-0.6) in M2G following 6 h of induction with 0.5 mM vanillate and quantified using MicrobeJ. ⁴⁰ Three biological replicates were performed to measure foci/cell from >150 cells. Error bars represent the standard error. Representative images in Figure S1.

(B) Colocalization patterns of the BR-body-enriched protein fusions with BR-body markers. Colored line traces indicate the pattern of localization observed for individual foci. The correlation was calculated for each line trace using the BR-body-enriched client as a reference, and each line trace correlation value was

Article



we used an RNase E depletion strain where the sole copy of RNase E is under control of the xylose promoter. 4 While most proteins maintained similar YFP fluorescence in the RNase E depletion strain, RhIB-YFP, Aconitase-YFP, PNPase-YFP, and RNase H1-YFP were too dim to detect (Figures 2C and S2). To overcome low Aconitase-YFP expression, we utilized a strain in which Aconitase-YFP is present at its native locus in the xylose-dependent RNase E depletion strain. 4 While most depletion strains would saturate cultures overnight, PNPase-YFP expression was toxic in the depletion background, leading to extremely slow cell growth in liquid culture making it impossible to assay. As a control we included PopZ, which is known to form an independent biomolecular condensate in Caulobacter. 6 For Aconitase, RNase D1, Hfq, and Rho, fluorescent foci decreased upon RNase E depletion, suggesting that these proteins require RNase E to assemble into foci. Interestingly, for MetK and RhIE, foci levels were unchanged or higher upon RNase E depletion, like the PopZ control, suggesting that these two proteins assemble into foci independent of RNase E. To examine whether these enriched proteins impact RNase E phase separation, we measured RNase E-GFP foci in strains where the enriched proteins were deleted. Due to Aconitase, RNase D1, and Rho being essential, we inserted RNase E-GFP into RhlB and Hfq deletion strains, or an RhIE disruption mutant strain. We observed no significant difference in the number of RNase E-GFP foci in these strains (Figure 2D), suggesting that RhIB, RhIE, and Hfg do not impact BR-body assembly in vivo.

As MetK and RhIE proteins were found to form RNase E-independent foci in vivo, we tested whether these proteins could directly self-assemble into condensates in vitro. In addition to MetK and RhIE, we also included several proteins from the BR-body enrichment dataset and proteins known to interact with RNase E (Figures 3 and S3A). Purified proteins were incubated at their estimated in vivo concentrations⁴¹ with or without 20 ng/μL of Caulobacter total RNA. We found that RhIE, DEAD, Hfg, and FabG assembled RNA-stimulated condensates in vitro (Figures 3A and 3B), suggesting that these proteins are scaffolds that can drive RNA-dependent condensation. MetK assembled smaller RNA-stimulated condensates, suggesting that it has a weaker capacity of RNA-dependent condensation. Conversely, most of the proteins tested, including PNPase, Aconitase, RhlB, RNase D1, Ribosomal protein S1, NudC, RppH, Rho, NusG, DnaK, and Tyrosyl tRNA synthetase (TyrRS), did not phase separate (Figure S3B). Consistent with the phase separation of RhIE, DEAD, and Hfq, the homologous proteins from E. coli were recently found to assemble into condensates in vitro or when overexpressed in vivo. 7,42 To test whether these structures are condensates, we performed high-salt and RNase treatment of pre-formed condensates (Figure 3C), and each condensate was strongly dissociated by either treatment, suggesting that multivalent electrostatic interactions with RNA are important for phase separation, like RNase E.4 RhIE, DEAD, and Hfq contain intrinsically disordered regions (IDRs) (Figure 3A) that have been characterized as important for their E. coli homologs' ability to phase separate. 42,43 Prior experiments also showed the IDR of RNase E was necessary and sufficient for phase separation.⁴ To test the IDRs' impact on phase-separation, we deleted the IDRs of Caulobacter RhIE, DEAD, and Hfq and tested RNA-dependent phase separation. FabG and MetK lacked IDRs and were not included. Hfq∆IDR and DEAD∆IDR showed reduced phase separation, while RhIEΔIDR was indistinguishable from wild-type (Figure S3C). Overall, this suggests that, for some scaffold proteins, IDRs promote but are not strictly required for phase separation.

A complex network of molecular interactions regulates **RNP** condensation

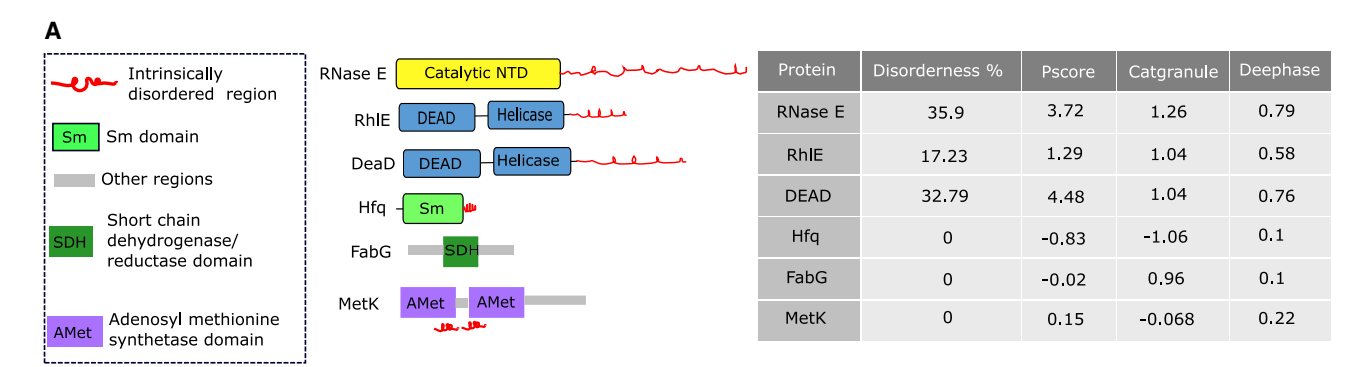
To understand which proteins can directly enter BR-bodies, we selected a set of 18 proteins (Figure S3A) to test for recruitment into RNase E droplets (Figure 4A). We picked proteins enriched from the BR-body proteomics dataset with known RNA-processing roles, proteins known to have protein-protein interactions with RNase E but not detected in the BR-body proteomics experiment, as well as negative control proteins with low BR-body enrichment and no known/predicted interaction with RNase E. In these experiments RNase E and RNA were mixed to form an RNase E condensate, followed by incubation with a Cv5-labeled test protein. The partition coefficient (PC) was calculated based on the Cy5 fluorescence (Figures 4B and S4A). We observed that the core RNA degradosome proteins PNPase, Aconitase, RhIB, and RNase D1 all had positive PCs ranging from 2.7 to 4.7, showing that they enter RNase E condensates, while our negative controls BSA and SpmX, which form a polar signaling condensate, 6 did not enter the RNase E condensate and yielded a PC near 1, indicating no enrichment. We also identified PCs at similar levels to the core degradosome proteins for RhIE, DnaK, and FabG. In contrast, NudC, RppH, Rho, NusG, and TyrRS all had PCs close to 1, like the negative controls BSA and SpmX (Figure 4B). The low PCs for RppH and NudC are consistent with their lack of enrichment in the BR-body proteomics assay; however, Rho, NusG, and TyrRS all had significant BR-body proteomic enrichment, suggesting they may enter BR-bodies indirectly through another protein. Despite the finding that many proteins were able to enter BR-bodies, none of these proteins altered

plotted as a single dot. More than 30 foci for each BR-body-enriched protein were used. The median value is represented as a black line. Statistics were calculated by a two-tailed t test with unequal variance.

(C) Subcellular localization patterns of Caulobacter YFP-fusion strains expressed from the vanA locus in the RNase E depletion background where the sole copy of the RNase E gene is controlled by the xylose promoter. A native gene fusion was used because Aconitase-YFP intensity was too low to measure when expressed from the vanillate promoter. The YFP intensity of each image was normalized from its brightest level relative to its background level. Depletion strains were grown to mid-exponential phase of growth (OD 0.3-0.6) and imaged after 24 h of xylose depletion. Quantitation of the number of Caulobacter protein-YFP foci/cell measured in M2G minimal medium with xylose (+Xyl) or lacking xylose (-Xyl). The squares represent the strains whose YFP levels were too low to visualize. All images were quantified using MicrobeJ. 40 Three biological replicates were used to calculate the average foci/cell with >175 cells. Error bars represent the standard error. Representative images in Figure S2.

(D) RNase E-GFP foci/cell were measured in wild-type, rhlB, rhlE, and hfq mutant backgrounds. Error bars represent the standard error from >100 cells. Scale bars, 1 μm.





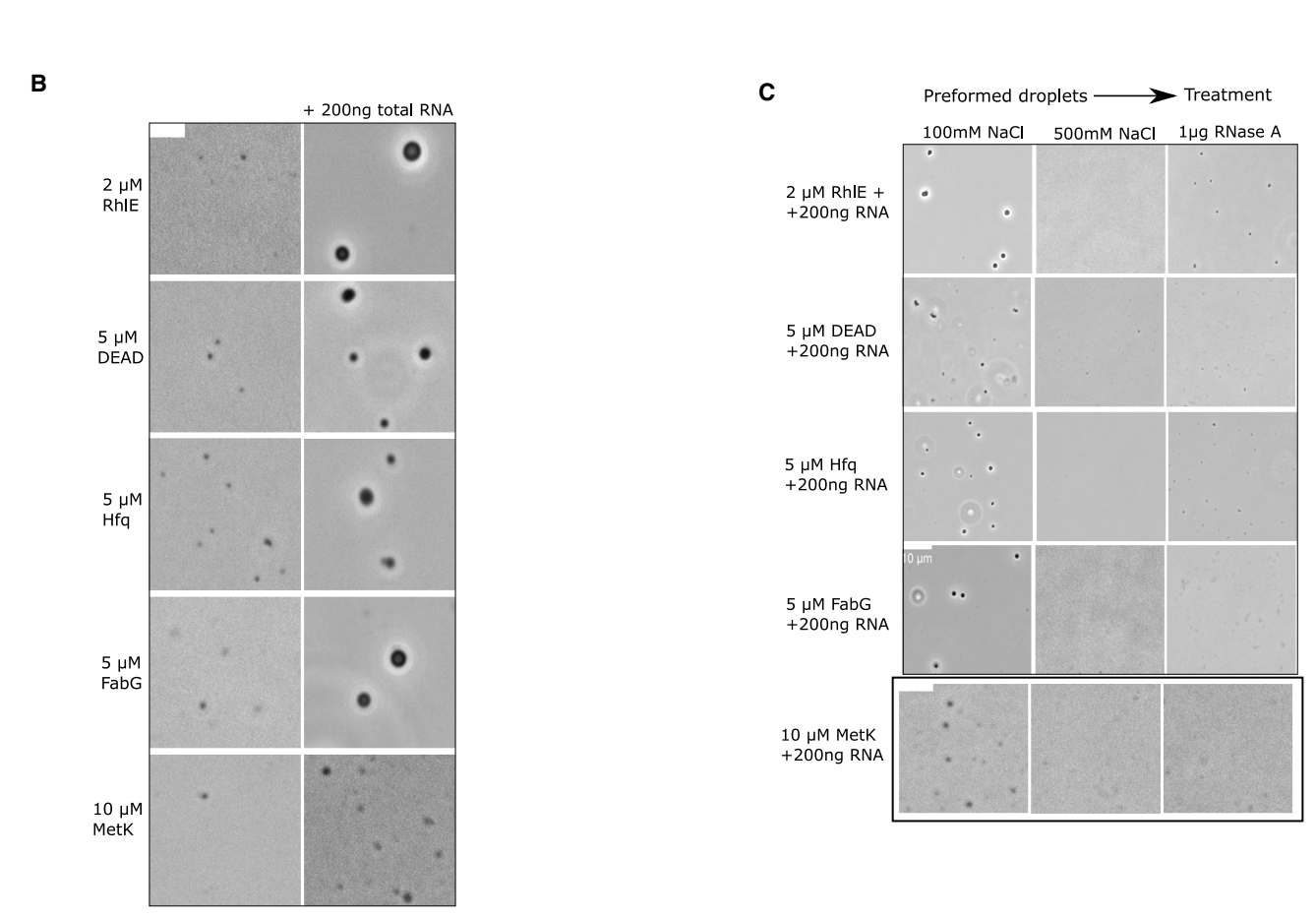


Figure 3. Some BR-body-enriched proteins can drive RNA-dependent biomolecular condensation

(A) Left: domain organization of proteins that undergo LLPS. The red line indicates disordered regions as predicted by PONDR. Right: prediction of the propensity to LLPS by Disorderness, ⁴⁴ Pscore, ⁴⁵ Catgranule, ⁴⁶ and DeePhase ⁴⁷ scores.

(B) Phase-contrast images of the purified proteins incubated at their in vivo concentrations: DEAD (5 μ M), Hfq (5 μ M), RhIE (2 μ M), FabG (5 μ M), MetK (10 μ M) in 20 mM Tris (pH 7.4), 100 mM NaCl, 1 mM DTT +/- 200 ng Caulobacter total RNA. Scale bars, 2 μ m.

(C) The dissolution of droplets was observed by adding either 0.5 M NaCl or RNase A (1 µg) to the preformed droplets. All the droplets were found to be NaCl and RNase sensitive. Scale bars, 10 µm for RhIE, DEAD, Hfq, and FabG, and 3 µm for MetK.

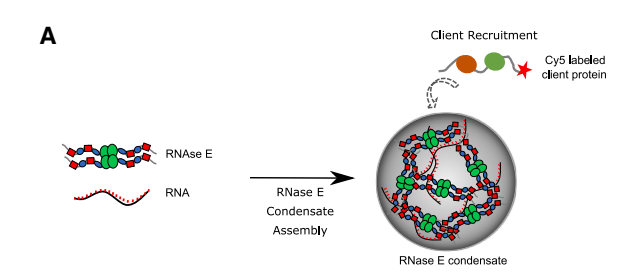
the PC of RNase E (Figure S4B), suggesting that most BR-body-associated proteins tested did not dramatically influence RNase E's condensation.

Next, we tested which BR-body-associated proteins might induce condensation in the absence of RNA (Figure S5A). We assessed the ability of BR-body-associated proteins to stimulate

RNase E condensation at their *in vivo* concentrations. ⁴¹ PNPase, RhlB, and RhlE stimulated RNase E condensates rather robustly in the absence of RNA (Figure S5A). In addition, FabG and Hfq stimulated irregularly shaped condensates in the absence of RNA, while Aconitase, RNase D1, NudC, RppH, Rho, NusG, DnaK, TyrRS, ribosomal protein S1, and MetK did not stimulate

Cell Reports Article





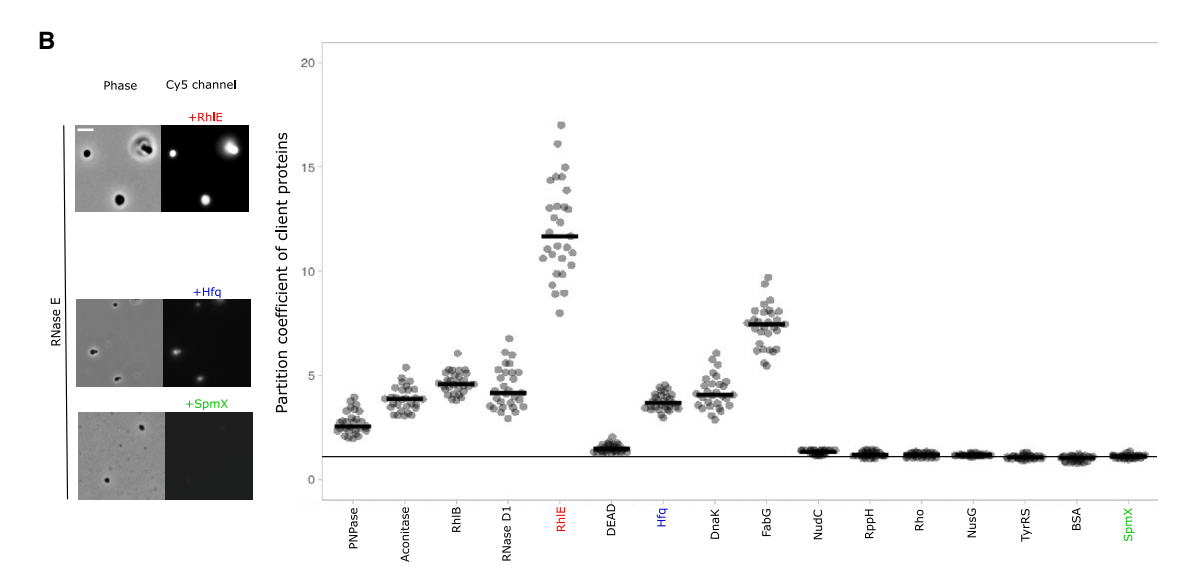


Figure 4. Many BR-body-associated proteins are directly recruited to RNase E condensates in vitro

(A) Cartoon showing the in vitro RNase E droplet recruitment assay. Cy5-labeled proteins are added to preformed RNase E CTD + RNA droplets to measure client partition coefficients (PCs).

(B) PC of Cy5-labeled client proteins in RNase E CTD (6 μM) + total RNA (200 ng). The black horizontal line through the plot indicates a PC of 1, which is the "no enrichment" baseline established by negative controls BSA and SpmX. PC of ribosomal protein S1 and MetK proteins could not be determined because they dissolved the droplets. The data are the average of three independent replicates and each dot in the graph represents a droplet. Median value is represented as a black line. The data were quantified in ImageJ software and plotted in PlotsofData. 48 Scale bar, 10 µm. Concentrations of proteins used to quantify PC: PNPase (5 μM), Aconitase (5 μM), RhIB (4 μM), RND (5 μM), DEAD(5 μM), Hfq (5 μM), DnaK (5 μM), FabG (5 μM), NudC (2.5 μM), RppH (1 μM), Rho (5 μM), NusG (5 μM), TyrRS (5 μ M), SpmX (5 μ M), and BSA (5 μ M).

RNase E condensation (Figure S5A). This suggests that a subset of BR-body-associated proteins can stimulate RNase E condensation independent of RNA.

Interestingly, we observed that the addition of ribosomal protein S1 or MetK, which were not BR-body enriched (Table S1) but were previously found to associate with RNase E via co-immunoprecipitation (co-IP),35 could dissolve RNase E droplets in vitro (Figures 4A and 5A). Ribosomal protein S1 could only dissociate the droplets if the condensates contained total RNA, while MetK showed strong dissolution if RNase E was condensed with RNA or with the protein PNPase. To test whether the differences between S1 and MetK were related to their inherent RNA binding interactions, we examined their apparent binding on 9S rRNA, a known RNase E substrate.³¹ Based on native gel shifts, we found that ribosomal protein S1 bound RNA with tighter apparent affinity than MetK (Figure 5B). The tighter apparent affinity with RNA may explain why ribosomal protein S1 preferentially dissolves RNase E condensates made with RNA. We also used an affinity pull-down assay to test MetK and ribosomal protein S1's association with MBP-RNase E. Indeed, compared with the core BR-body protein Aconitase, which can stoichiometrically bind to RNase E,30 we found that MetK showed less pull-down than Aconitase, while ribosomal protein S1 showed no detectable retention (Figures 5C and S5B). Overall, these data suggest that MetK dissociates BR-bodies through interactions with RNase E (Figure 5). Because MetK showed a weak pull-down signal, we tested the pairwise interaction between MetK and RNase E in a bacterial two-hybrid assay where each protein was expressed in E. coli49 and found that MetK and RNase E do interact (Figure 5D). In the bacterial two-hybrid assay, we found that Aconitase-T18/RNase E-T25 and MetK-T18/RNAse E-T25 interact similarly to the T18-Zip/T25-Zip positive control, and that RNase E-T25/S1-T18 showed no lacZ signal, like the T18/ T25 negative control. To examine whether the observed in vitro dissolution effect of S1 and MetK on BR-bodies is relevant



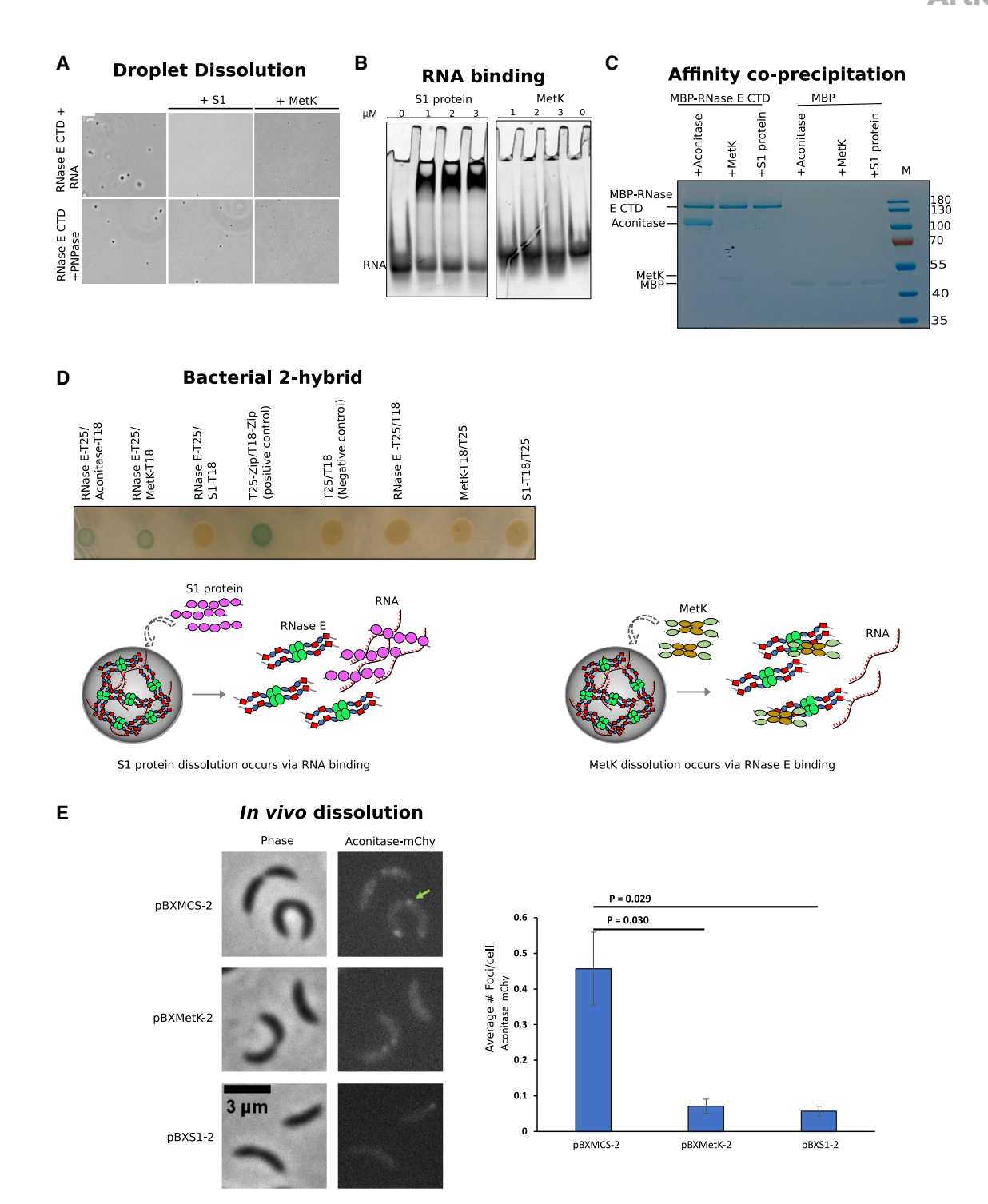


Figure 5. Ribosomal protein S1 and MetK dissolve BR-bodies in vitro and in vivo

(A) Images of in vitro RNase E droplets incubated with either S1 or MetK. Scale bar, 10 µm. RNA-induced RNase E droplets are shown at the top and PNPaseinduced RNase E droplets are shown below. Concentrations used were: RNase E CTD (10 µM), S1 (5 µM), MetK (5 µM), PNPase (5 µM), and total RNA (20 ng/µL). (B) RNA and protein binding data for S1 and MetK with 1 µM RNA. RNA was visualized by SYBR Gold staining.

(C) Aconitase and MetK pull-down with RNase E. RNase E-CTD-MBP or MBP (negative control) (5 μ M) were incubated with 5 μ M of Aconitase or 15 μ M of MetK or 15 μ M of S1 protein. Eluates were resolved on 10% SDS-PAGE.

(legend continued on next page)

Article



in vivo, we inserted the ribosomal protein S1 rpsA and metK genes into the pBXMCS-2 overexpression vector⁵⁰ and transformed the plasmid into Caulobacter harboring a BR-body marker (Aconitase-mCherry).4 We observed in vivo that both MetK and ribosomal protein S1 overexpression strongly reduced Aconitase-mCherry foci (Figure 5E).

Some BR-body-enriched proteins were able to assemble into distinct RNP condensates independent of RNase E (Figure 3B), but their client specificity was unknown. Because the RNA degradosome client proteins are known to be stoichiometrically bound to RNase E via direct protein-protein interaction sites^{31,35} and show strong colocalization with BR-bodies (Figure 2B), we tested the specificity of each driver/scaffold to each core RNA degradosome protein labeled with Cy5 dye (Figure 6A). We observed a larger PC for all Cy5 degradosome clients to RNase E condensates compared with the other scaffolds/drivers (Figures 6A and S5B), suggesting that the degradosome proteins have a specificity for entering RNase E condensates.

Next, the miscibility of the drivers/scaffolds of each single RNP condensate was examined (Figure 6B). First, we pre-formed a condensate using an unlabeled scaffold and then added in a Cy5-labeled scaffold in all pairwise combinations and assayed the PCs. We induced condensation in the presence or absence of RNA to test the RNA dependency of each interaction. In the presence of RNA, we assayed condensate formation using the predicted in vivo protein concentrations, 41 and, in the absence of RNA, condensates were stimulated by increasing the protein concentration above its in vivo concentration. For the RNase E condensate, we observed similar recruitment of other scaffolds regardless of whether the condensates were formed with RNA or protein only (Figures 6B and S5C). The PCs for these scaffolds into RNase E condensates correlated with the BR-body enrichment measured previously. RhIE was recruited most strongly into the RNase E condensate (11 PCs) and had the highest BR-body enrichment (10-fold). RhIE was followed by Hfq (7.5 PCs, 3.2-fold BR-body enrichment), FabG (3.8 PCs, 2.2-fold BR-body enrichment), and DEAD (1.5 PCs, 1.6-fold BR-body enrichment). RhIE was recruited strongly into other RNP condensates, with PCs ranging from 4.3 to 11, while the other scaffolds were recruited poorly into RhIE-RNA condensates, with PCs ranging from 1.5 to 2.5. In the absence of RNA, RhIE strongly recruited RNase E (12 PCs) or DEAD (9.8 PCs), while Hfq and FabG maintained similar PCs (Figure S5C). DEAD condensates showed strong recruitment of RhIE and lower recruitment of the other scaffolds, with subtle changes in the presence or absence of RNA. RhIE and FabG were similarly recruited to Hfg condensates regardless of the presence of RNA. RNase E dissolved Hfq-RNA condensates, while Hfq protein-only condensates strongly recruited RNase E (6.9 PCs). DEAD was recruited at a low level in Hfq-RNA condensates (1.8 PCs) and dissolved Hfq-only condensates. FabG condensates only formed in the presence of RNA and showed the strongest recruitment of RhIE (7.4 PCs) and Hfq (3.4 PCs). In summary, the scaffold proteins that assemble diverse RNP condensates show specificity of recruitment, suggesting that some RNP condensates can intermix while others do not.

The asymmetric recruitment/dissolution (Figure 6B) and specificity of clients (Figure 6A) observed may help shape the composition of the heterogeneous RNP condensates observed in the cell (Figure 2B). We chose to study the RhIE-RNase E pair further because it showed the strongest directional recruitment in the presence of RNA (Figure 6B). Specifically, RhIE was recruited robustly into RNase E droplets, but RNase E was poorly recruited into RhIE droplets. We altered the order of addition of RhIE and RNase E before triggering phase separation (Figure 6C). If the proteins were mixed before condensation with RNA, we observed that RNase E and RhIE mix uniformly. However, when each protein was pre-assembled into a condensate with RNA before mixing both RNP condensates together, we observed that RNase E and RhIE condensates did not readily mix (Figure 6C). This contrasts with the prior observation that free RhIE readily entered RNase E condensates (Figure 6B), suggesting that the order of assembly influences the composition of RNase E and RhIE condensates.

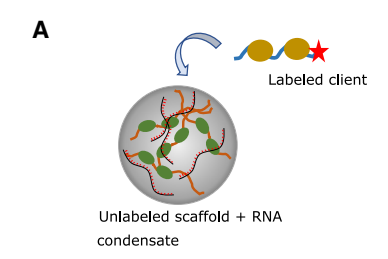
To examine the order of RNase E and RhIE condensate formation in vivo, we took time-lapse movies of RhIE and RNase E foci formation in cells. As a positive control, we observed that RNase E-YFP and the core degradosome protein Aconitase-mCherry foci appear simultaneously (Figures 6D and S6A) with uniform colocalization. When BR-bodies appear first, as indicated by Aconitase-mCherry foci, we regularly observed RhIE-YFP signals within these foci (Figure 6D), consistent with the ability of RNase E condensates to recruit RhIE in vitro (Figure 6B). In contrast, RhIE-YFP foci that appeared first generally lacked a colocalized Aconitase-mCherry focus, consistent with the lack of in vitro recruitment of RNase E by RhIE (Figure 6B). Taken altogether, these observations suggest that the molecular interactions driving RhIE and RNase E condensation control the ability of these condensates to co-assemble and mix. To further test whether the material properties of RhIE and RNase E condensates affect mixing, we performed in vitro FRAP on RhIE and RNase E droplets (Figure S6B). We observed that RNase E rapidly recovers either in RNase E-RNA condensates or in mixed RNase E-RhIE-RNA condensates, while RhIE showed little to no recovery in either RhIE-RNA condensates or RNase E-RhIE-RNA condensates (Figure S6B). This suggests that the more dynamic exchange in RNase E droplets compared with RhIE droplets contributes to the preferred directional RhIE to RNase E assem-

As RNase E did not appear to readily enter other associated RNP condensates (Figure 6B), we wanted to better understand the role of RNA and the associated degradosome proteins on

⁽D) Bacterial two-hybrid assay showing the spots of BTH101 cells cotransformed with plasmids expressing the proteins as indicated in the figure. Blue spots represent an interaction between the two proteins. The positive control pairs were RNase E-T25/Aconitase-T18 and T25-Zip/T18-Zip. Underneath is a proposed cartoon of the RNA dependence of droplet dissolution by S1 and MetK.

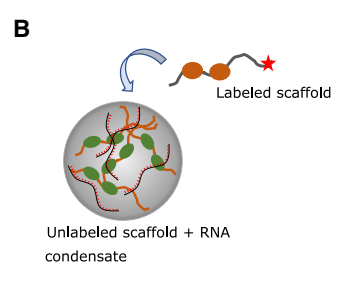
⁽E) BR-bodies (marked with Aconitase-mCherry) are dissolved upon overexpression of ribosomal protein S1 or MetK from the pBX multicopy plasmid. Quantitation of the average Aconitase-mCherry foci/cell was performed using MicrobeJ. Error bars represent the standard error. More than 700 cells were used for each analysis.



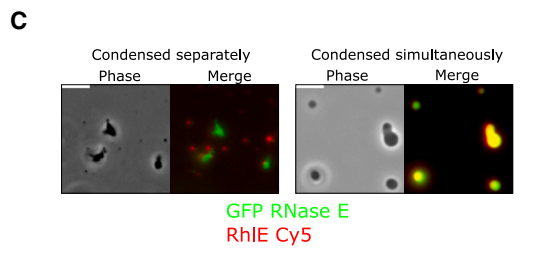


Labeled client					
Scaffold	RhlB	PNP	Aco	RNase D	
RNase E	4.7	2.6	4	4	
RhlE	1.0	1.0	1.0	1.0	
DEAD	1.5	1.5	1.5	1.5	
Hfq	2.3	1.7	2.5	1.7	
FabG	1.5	1.7	1.5	1.6	

Partition Coefficient			
	15	High	
	10		
	5		
	1	Low	



Labeled Scaffold					
Scaffold	RNase E	RhIE	DEAD	Hfq	FabG
RNase E	Х	11	1.5	7.5	3.8
RhlE	1.6	X	1.5	2.5	2.5
DEAD	1.7	7.6	Х	3.3	2.6
Hfq	ND	4.3	1.8	Х	2.4
FabG	1.9	7.4	1.5	3.4	Х



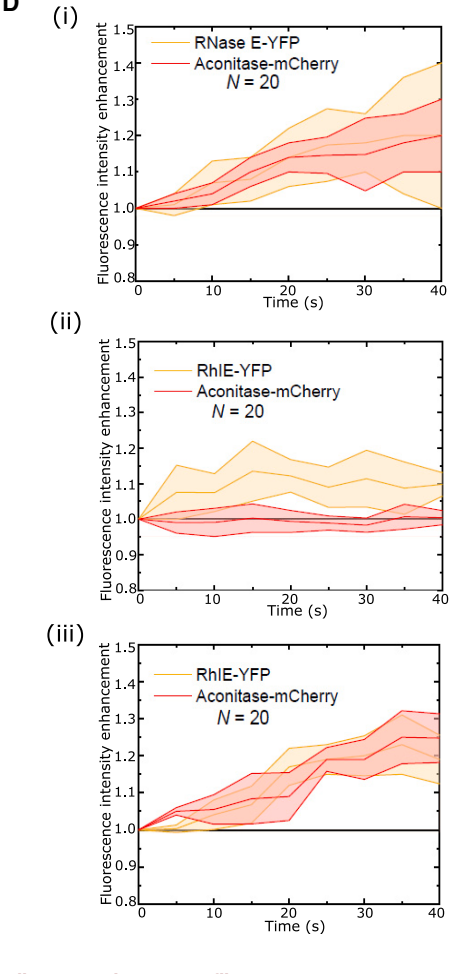


Figure 6. BR-body-associated drivers have distinct condensation and client recruitment profiles

(A) Scaffold proteins recruit a distinct subset of client proteins. Each RNA degradosome client, labeled with Cy5, was tested for recruitment into pre-formed condensates of each BR-body-associated scaffold indicated on the left. Each protein scaffold was incubated with RNA and allowed to phase separate. Then a small concentration of Cy5-labeled proteins was tested for entry into the condensate by measuring the partition coefficients (PCs) of the Cy5 channel. The value is a median of three independent replicates of >50 droplets each. The data were quantified in ImageJ. Concentrations of the scaffolds used for making condensates

Article



RNase E condensation. We therefore examined the kinetics of condensation via time-lapse microscopy (Figures 7A and 7B). This assay likely reflects the kinetic processes of phase separation and surface wetting of the microscope slide. When incubated alone at its cellular concentration, RNase E did not phase separate in vitro even after long incubations of many minutes. The addition of RNA strongly stimulated the rate of condensation, occurring on the sub-minutes timescale, consistent with the known importance of RNA for RNase E condensation in vivo and in endpoint in vitro assays. 4,29 When RNase E was incubated at concentrations much higher than its cellular concentration, it was able to phase separate without RNA after many minutes (Figure S7A).

RNase E is known to scaffold the RNA degradosome protein complex, and the degradosome proteins stoichiometrically bind to RNase E³¹ and are homogeneously present with RNase E in BR-bodies.4 To test the effects of degradosome proteins on condensation kinetics, we added either PNPase or the full set of core-degradosome proteins (PNPase, Aconitase, RhIB, and RNase D1) to the condensation assembly experiment. Upon the addition of PNPase or the full set of core RNA degradosome proteins, RNase E still rapidly condensed on a sub-minutes timescale that was accelerated by the addition of RNA (Figures 7A and S7B). This suggests that the combined interactions with the RNA degradosome proteins likely do not dramatically alter RNase E's condensation kinetics with RNA. This may be due to the degradosome protein binding sites being located outside the Arg-rich RNA binding sites in the C-terminal domain of RNase E.31 As noted previously, we observed that the degradosome protein PNPase was able to stimulate RNase E condensation in vitro without RNA (Figure S5A). We therefore assayed the kinetics of RNase E and PNPase condensation without RNA and found that the kinetics were dramatically slower than with RNA (Figures 7A and S7B). Overall, this suggests that RNA provides the strongest kinetic stimulation of condensation, and that the RNA degradosome clients can provide a slight further enhancement of RNA-mediated condensation kinetics.

To understand if RNA or degradosome protein interactions alter the mobility of molecules in the condensed state, we performed FRAP experiments (Figures 7B and 7C). RNase E condensates lacking RNA had the slowest recovery, at 2.4 min $\tau_{1/2}$, while the addition of RNA accelerated the FRAP recovery $\tau_{1/2}$ to 0.23 min. Interestingly, mobility was still fast upon the addition of PNPase and RNA or all core-degradosome proteins and RNA, with recovery times similar to the RNase E with RNA sample ($\tau_{1/2}$ of 0.34 and 0.42 min, respectively). This suggests that the addition of RNA significantly increases the mobility of RNase E condensates, regardless of the presence of degradosome clients. Interestingly, the addition of RNase E and PNPase in the absence of RNA showed a recovery $\tau_{1/2}$ of 0.38 min. This suggests that, even though the core-degradosome proteins do not dramatically stimulate the rate of condensation, degradosome protein interactions likely do influence the mobility of RNase E within the droplets, either indirectly by altering the structure of the CTD or directly by influencing multivalent protein-protein interactions in the condensed state. Altogether, RNA stimulates the rate of RNase E condensation, while the recruitment of RNA or protein clients increases the mobility of RNase E within the condensate, which may promote enhanced biochemical activity.

DISCUSSION

A complex protein interaction network impacts BR-body condensation and composition

Analysis of the BR-body proteome revealed enrichment of >100 proteins of various biochemical functions, suggesting that BRbodies are more complex than previously assumed. We observed that a subset of BR-body-enriched proteins known to stoichiometrically assemble into the RNA degradosome (RNase E, RhIB, Aconitase, and PNPase) appear to be uniformly enriched in BR-bodies in vivo4 and selectively recruited to RNase E condensates in vitro (Figure 6). This suggests that the RNA degradosome likely composes the "core" set of proteins making up each BR-body. As observed for yeast P-bodies, a set of "core" proteins that were found to be quantitatively enriched²⁷ and likely homogeneously represented in these structures, were successfully reconstituted in vitro with similar dynamics properties and stoichiometries identified.²⁸ An important future goal will be to define the role of BR-body localization to each of the core enzymes involved in the RNA decay process. Indeed, in a two-protein BR-body system using only RNase E and PNPase, PNPase activity was observed to be directly stimulated by condensation with RNase E, 17 suggesting that the organization in BR-bodies may help to stimulate RNA degradosome activity.

In addition to a uniformly enriched core of RNA degradosome proteins, we also found multiple proteins that were heterogeneously localized with BR-bodies, including the DEAD-box

were: RNase E (6 μM), RhIE (5 μM), DEAD (5 μM), Hfq (5 μM), and FabG (10 μM). Concentrations of the labeled clients added were: RhIB (4 μM), PNP (5 μM), Aconitase (5 µM), and RND (5 µM),

⁽B) BR-body-associated scaffolds drive a complex network of dependencies controlling phase separation. Each protein scaffold was incubated with RNA and allowed to phase separate. Then a small concentration of Cy5-labeled proteins was tested for entry into the condensate by measuring the PC of Cy5 fluorescence. Concentrations of the scaffolds used for making condensates were: RNase E (6 μM), RhIE (5 μM), DEAD (5 μM), Hfq (5 μM), and FabG (10 μM). Concentrations of Cy5-labeled scaffolds were: RNase E (1 μM), RhIE (0.5 μM), DEAD (1 μM), Hfq (1 μM), and FabG (1 μM).

⁽C) Order of assembly experiments using GFP-RNase E (6 μM) and RhIE-Cy5 (5 μM) condensates. "Condensed simultaneously" indicates that both proteins were added together before the addition of RNA (20 ng/µL) to trigger condensation. "Condensed separately" indicates that both proteins were incubated with RNA (20 ng/µL) yielding separate condensates that were then mixed.

⁽D) In vivo order of foci assembly. Time-lapse two-color imaging of RhIE-YFP and Aconitase-mCherry proteins was performed and the evolution of the intensity of each focus after formation is plotted. (i) Intensity evolution in cells in which both Aconitase-mCherry and RhIE-YFP condensates are formed simultaneously. The middle line indicates the average and the colored region represents the standard deviation between all three replicates. (ii) Cells in which RhIE-YFP condensates were formed first and the subsequent appearance of Aconitase-mCherry in RhIE-YFP condensates was tracked. (iii) Cells in which Aconitase-mCherry condensates were formed first and the subsequent appearance of RhIE-YFP in Aconitase-mCherry condensates was tracked.



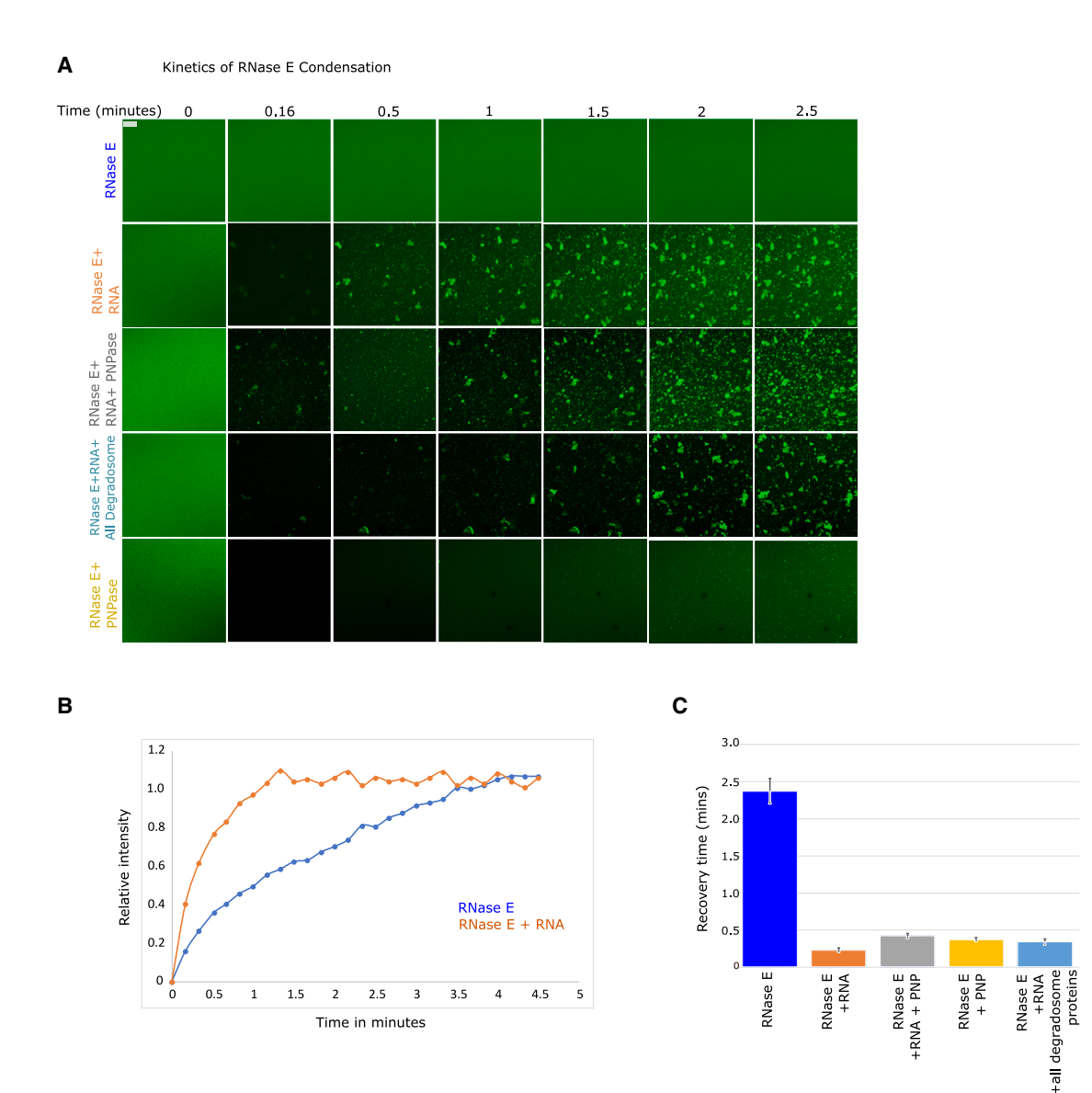


Figure 7. RNA stimulates rapid BR-body condensation in vitro

(A) Time-lapse imaging of RNase E CTD YFP (RCY) condensate formation. RCY (6 µM) assembly was monitored either alone or with different combinations of 100 ng/μL RNA, 5 μM PNPase, or all degradosome proteins (5 μM PNPase, 4 μM RhlB, 5 μM RNase D1, and 5 μM Aconitase) as indicated on the left. Scale bar, $20 \ \mu m$. Representative images from one of three replicates are shown.

(B) FRAP recovery of RNase E condensates and RNase E + RNA condensates, plotted in MS Excel. FRAP recovery is averaged from ten droplets.

(C) Apparent FRAP recovery for droplets with the indicated composition. Because no RCY condensates were present at 6 µM without RNA, the concentration was increased to 30 μM to induce condensates. The values are averages from >6 droplets, and the error bars represent the standard deviation.

RNA helicase RhIE, the transcription termination factor Rho, and the RNA chaperone Hfq. Although Rho was strongly colocalized with RNase E foci in vivo, we found that only a subset of RNase E foci contained Rho signal (Figure 2). RhIE and Hfg were both present in a subset of RNase E foci, and they could also form independent foci in vivo that did not contain RNase E (Figure 2). Importantly, non-RNase E scaffolds that can undergo heterotypic phase separation with RNA are enriched in BR-bodies, which suggests that many cellular RNP condensates exist and interact with BR-bodies. Five proteins that interact with RNase E were

identified as scaffolds that can phase separate with RNA in vitro: RhIE, DEAD, Hfq, FabG, and MetK. Together with the RNApol and Rho condensates identified previously, 5,51 this suggests that bacteria contain many RNP condensates that likely help coordinate multi-step reactions in RNA processing.3

DEAD-box RNA helicases appear to be important players in biomolecular condensates, 42,52 and we observed three enriched in BR-bodies. We observed that RhIE and DEAD act as scaffolds that undergo RNA-dependent phase separation in vitro, while RhIB cannot phase separate alone, but can enter the BR-body

Article



through RNase E's IDR, like that observed for E. coli homologs, 42 suggesting that phase separation is a conserved feature of these helicases. Interestingly, we observed strong recruitment of RhIE and RhIB into RNase E condensates, but DEAD was observed to be recruited to a lower extent (Figure 4). While RhIB was strongly colocalized with RNase E4 and RhlB foci dissociated in cells after RNase E depletion, RhIE showed heterogeneous, partially overlapping localization with RNase E and remained localized in foci even after RNase E depletion (Figure 2). The function of DEADbox proteins in BR-bodies is not well understood; however, RhIE becomes more highly expressed when Caulobacter is grown in the cold,35 which may alter the composition and function of BR-bodies under these conditions.

BR-body proteomics identified Hfq as a BR-body-enriched protein. Hfq chaperones small-RNAs to target mRNAs to repress translation/induce decay. 53-57 It is unsurprising that Hfg was enriched in BR-bodies because the BR-body transcriptome is highly enriched with poorly translated mRNAs and small-RNAs.²⁹ Hfq phase separates with RNA in vitro and forms heterogeneous colocalized foci in Caulobacter. E. coli Hfg was recently found to phase separate with DNA, polyphosphate, 43 and RNA, 10 and its condensation is promoted in vitro by its intrinsically disordered CTD. 43 E. coli Hfq foci were previously identified to colocalize with RNase E in nitrogen-starved E. coli cells, and, while Hfg is not a core member of the E. coli or Caulobacter RNA degradosome, it has been found to associate with RNase E in multiple species.⁵⁸ Interestingly, we observed that Caulobacter Hfq is readily recruited into RNase E-RNA condensates, but RNase E was not recruited into Hfq-RNA condensates, suggesting a preferred directionality in condensate mixing. E. coli Hfg condensates promote sRNA-mRNA annealing¹⁰ and RNase E IDR mutants prevent sRNA-mRNA silencing.⁵⁹ These RNase E IDR mutants were later found to prevent BR-body phase separation.⁴ Therefore, the coordination of Hfq with BR-bodies likely helps degrade silenced mRNAs; the same function has been proposed for miRNA/siRNA/LSM in P-bodies.²²

The BR-body-associated proteins identified that can dissolve BR-bodies, ribosomal protein S1 and MetK, may play important regulatory roles in controlling BR-body assembly. Ribosomal protein S1 appears to dissolve RNase E condensates via its RNA binding capacity, while MetK appears to dissolve RNase E via protein-protein interaction with RNase E (Figure 5). Ribosomal protein S1 is present in a ribosome-bound and a ribosome-free form; it unfolds structured mRNAs in preparation for translation initiation 60 and protect mRNAs from RNase E-dependent decay.⁶¹ Since BR-bodies and ribosomes compete for mRNA substrates, 4 ribosomal protein S1 may prevent BR-body condensation on highly translated mRNAs by locally disrupting RNase E condensation when in polysomes. Alternatively, if ribosomal protein S1 dissociates from the ribosome, it may be able to globally dissolve BR-bodies, potentially acting as a sensor of translation. We found that MetK, an essential enzyme producing S-adenosylmethionine, can phase separate with RNA. MetK was previously found to bind RNase E in cells grown in the cold, 35 and we identified a protein-protein interaction between RNase E and MetK under normal growth temperature (Figures 5 and S5C), suggesting that MetK likely inhibits RNase E condensation directly by blocking multivalent interactions with RNase E or indirectly by altering the conformation of RNase E. Despite its rather weak RNA binding observed in vitro, Caulobacter MetK phase separated in the presence of RNA, and homologs from S. meliloti and E. coli were identified to bind RNA.⁶² Because MetK is the sole enzyme creating S-adenosylmethionine in Caulobacter, perhaps it might act as a metabolic sensor that could tune the number of BR-bodies to carbon availability. In line with this hypothesis, MetK protein levels are dramatically altered upon carbon starvation.63

RNA is critically important to BR-body condensation

Reconstitution of minimal BR-body cores revealed that RNA, which was hypothesized to play a key role in BR-body assembly in vivo, 4 plays a key role in BR-body assembly in vitro. We observed that RNA can kinetically stimulate the rate of BRbody condensation on the sub-minutes timescale (Figure 7), further suggesting that the main cause of RNase E's robust foci dissolution under rifampicin treatment is the RNA depletion induced by rifampicin and not other cellular perturbations, such as nucleoid expansion.⁶⁴ The addition of RNA degradosome proteins does not alter the rate of RNase E condensation, but it does appear to enhance RNase E mobility by FRAP (Figure 7). In vivo, the RNA in BR-bodies are long, poorly translated mRNAs and small-RNAs; BR-bodies are depleted of rRNA and other highly structured ncRNAs.²⁹ This suggests that, at least under logarithmic growth conditions, the availability of poorly translated RNA helps catalyze rapid BR-body assembly. Interestingly, BR-bodies could be induced with some client proteins in the absence of RNA, such as PNPase; however, the rate of the condensation was far slower than with RNA. While likely not relevant under log growth conditions where BR-bodies have subminutes dynamics,4 such assemblies might occur under nongrowing conditions, such as stationary phase.

The identification of five RNP condensates associated with BR-bodies suggests that condensates have a broader role in bacterial cell organization than previously anticipated. Indeed, recent high-throughput methods designed to detect proteins crosslinked to RNA identified >1,100 RNA binding proteins in E. coli, including many metabolic enzymes. 65,66 Similarly, we identified two metabolic enzymes, MetK and FabG, that have the capacity to phase separate with RNA (Figure 3). While the ability of metabolic enzymes to bind to RNA is referred to as "moonlighting" RNA binding activity, 67 it is possible that, due to the large number of RNA binders, RNP condensates play a broad role in organizing metabolic pathways in the bacterial cytoplasm. Because studies to identify and characterize condensates are time-intensive, bioinformatic prediction of proteins that phase separate is the only method that can be utilized across proteomes. However, the current algorithms 47,68 do not accurately predict the phase separation of all five of the proteins identified. Perhaps current phase separation prediction algorithms rely too much on IDR predictions, which often affect phase separation, but are not always required. 69 When developing next-generation algorithms to predict phase separation, it will be important for training datasets to include bacterial phase separating proteins to improve their predictive power.





Limitations of the study

While BR-body enrichment followed by LC-MS found many direct interactors with RNase E, we have identified multiple proteins that cannot directly enter RNase E CTD droplets in vitro. For example, transcription proteins Rho and NusG are highly enriched proteins, yet were unable to enter purified RNase E CTD-RNA condensates. We hypothesize that these proteins may enter BR-bodies through an unidentified BR-body-enriched protein/RNA or the catalytic NTD of RNase E. While we identified five condensates in Caulobacter, MetK exhibited small droplets in the presence of RNA, suggesting that it has a weak capacity to phase separate. In addition, MetK weakly associated with RNase E by pull-down and bacterial two-hybrid assay, suggesting that it has a weak affinity for RNase E. More studies will be required to identify the binding sites between MetK and RNase E and to quantitatively measure their binding affinity to each other. For all five identified condensates, it will be important to examine their dynamic properties in vivo and to probe their cellular and biochemical functions.

STAR*METHODS

Detailed methods are provided in the online version of this paper and include the following:

- KEY RESOURCES TABLE
- RESOURCE AVAILABILITY
 - Lead contact
 - Materials availability
 - Data and code availability
- EXPERIMENTAL MODEL AND STUDY PARTICIPANT DE-**TAILS**
 - Caulobacter crescentus
- METHOD DETAILS
 - Plasmid construction
 - Bacterial 2 hybrid plasmids
 - O Strains used in bacterial two-hybrid assay
 - O BR-body enrichment assay and LC-MS proteomics
 - In vivo localization of BR-body associated proteins
 - O RNase E depletion
 - Colocalization of YFP tagged foci forming proteins with BR-body markers
 - O In vivo localization of RNase E-GFP foci in the strains with BR-body enriched proteins deleted
 - Dissolution of MetK and ribosomal protein S1
 - Cell imaging
 - RNA extraction
 - Protein purifications
 - O Cyanine 5 protein labeling
 - O In vitro phase separation experiments and droplet as-
 - In-vitro protein pull down assay
 - Electrophoretic mobility shift assay
 - Bacterial two-hybrid assay
 - O Determination of the assembly order of RhIE, RNase E, and aconitase foci
 - Condensate growth kinetic assays
- QUANTIFICATION AND STATISTICAL ANALYSIS

- Foci quantification
- Colocalization analysis
- FRAP assays

SUPPLEMENTAL INFORMATION

Supplemental information can be found online at https://doi.org/10.1016/j. celrep.2023.113229.

ACKNOWLEDGMENTS

The authors acknowledge the support of NIH grant R35GM124733 to J.M.S., NIH grants R01GM143182 and R01GM144731 to J.S.B., NIH grant R01GM136863 to W.S.C., NSF grant CMMI-1914436 to Y.Z., and NIH grant R01GM139277 to M.C. We would like to acknowledge the Mass Spectrometry and Proteomics Facility at Notre Dame. Caulobacter cell and protein icons in the graphical abstract were created with Biorender.com. The authors thank Vincent Lawal for help with bacterial two-hybrid assays. The authors thank Erin Schrader for critical feedback.

AUTHOR CONTRIBUTIONS

V.N. performed protein purifications, all in vitro experiments, bacterial twohybrid assay, and in vivo experiments. I.W.R.-M. performed protein purifications, in vivo expression, depletion, and colocalization experiments, and made plasmids and strains for in vivo experiments. V.N., A.H., and J.V. performed droplet kinetic assays and FRAP experiments. A. Gega and M.C. made some plasmids. K.S.M., H.Y., and A. Ghosh purified proteins. N.S.M. purified BR-bodies for BR-body proteomics. C.B.M. and M.M.C. performed LC-MS data collection and analysis. L.A.O.-R. performed RhIE in vivo assembly experiments. J.M.S., M.M.C., J.S.B., Y.Z., and W.S.C. obtained funding and advised trainees on acquisition and analysis of the data. V.N., I.W.R.-M., and J.M.S. wrote the paper.

DECLARATION OF INTERESTS

The authors declare no competing interests.

Received: February 17, 2023 Revised: July 16, 2023 Accepted: September 22, 2023 Published: October 19, 2023

REFERENCES

- 1. Azaldegui, C.A., Vecchiarelli, A.G., and Biteen, J.S. (2021). The emergence of phase separation as an organizing principle in bacteria. Biophys. J. 120, 1123-1138. https://doi.org/10.1016/j.bpj.2020.09.023.
- 2. Banani, S.F., Lee, H.O., Hyman, A.A., and Rosen, M.K. (2017). Biomolecular condensates: organizers of cellular biochemistry. Nat. Rev. Mol. Cell Biol. 18, 285-298. https://doi.org/10.1038/nrm.2017.7.
- 3. Nandana, V., and Schrader, J.M. (2021). Roles of liquid-liquid phase separation in bacterial RNA metabolism. Curr. Opin. Microbiol. 61, 91-98. https://doi.org/10.1016/j.mib.2021.03.005.
- 4. Al-Husini, N., Tomares, D.T., Bitar, O., Childers, W.S., and Schrader, J.M. (2018). α-Proteobacterial RNA Degradosomes Assemble Liquid-Liquid Phase-Separated RNP Bodies. Mol. Cell 71, 1027-1039.e14. https://doi. org/10.1016/j.molcel.2018.08.003.
- 5. Ladouceur, A.-M., Parmar, B.S., Biedzinski, S., Wall, J., Tope, S.G., Cohn, D., Kim, A., Soubry, N., Reyes-Lamothe, R., and Weber, S.C. (2020). Clusters of bacterial RNA polymerase are biomolecular condensates that assemble through liquid-liquid phase separation. Proc. Natl. Acad. Sci. USA 117, 18540-18549. https://doi.org/10.1073/pnas.2005019117.
- 6. Lasker, K., von Diezmann, L., Zhou, X., Ahrens, D.G., Mann, T.H., Moerner, W.E., and Shapiro, L. (2020). Selective sequestration of signalling proteins

Article



- in a membraneless organelle reinforces the spatial regulation of asymmetry in Caulobacter crescentus. Nat. Microbiol. 5, 418-429. https://doi.org/ 10.1038/s41564-019-0647-7.
- 7. McQuail, J., Switzer, A., Burchell, L., and Wigneshweraraj, S. (2020). The RNA-binding protein Hfq assembles into foci-like structures in nitrogen starved Escherichia coli. J. Biol. Chem. 295, 12355-12367. https://doi. org/10.1074/jbc.RA120.014107.
- 8. Monterroso, B., Zorrilla, S., Sobrinos-Sanguino, M., Robles-Ramos, M.A., López-Álvarez, M., Margolin, W., Keating, C.D., and Rivas, G. (2019). Bacterial FtsZ protein forms phase-separated condensates with its nucleoidassociated inhibitor SImA. EMBO Rep. 20, e45946. https://doi.org/10. 15252/embr.201845946.
- 9. Wang, H., Yan, X., Aigner, H., Bracher, A., Nguyen, N.D., Hee, W.Y., Long, B.M., Price, G.D., Hartl, F.U., and Hayer-Hartl, M. (2019). Rubisco condensate formation by CcmM in β-carboxysome biogenesis. Nature 566, 131-135. https://doi.org/10.1038/s41586-019-0880-5.
- 10. Goldberger, O., Szoke, T., Nussbaum-Shochat, A., and Amster-Choder, O. (2022). Heterotypic phase separation of Hfq is linked to its roles as an RNA chaperone. Cell Rep. 41, 111881. https://doi.org/10.1016/j.celrep. 2022.111881.
- 11. Feng, Z., Chen, X., Wu, X., and Zhang, M. (2019). Formation of biological condensates via phase separation: Characteristics, analytical methods, and physiological implications. J. Biol. Chem. 294, 14823-14835. https://doi.org/10.1074/jbc.REV119.007895.
- 12. Mittag, T., and Pappu, R.V. (2022). A conceptual framework for understanding phase separation and addressing open questions and challenges. Mol. Cell 82, 2201-2214. https://doi.org/10.1016/j.molcel.2022. 05.018.
- 13. Kar, M., Dar, F., Welsh, T.J., Vogel, L.T., Kühnemuth, R., Majumdar, A., Krainer, G., Franzmann, T.M., Alberti, S., Seidel, C.A.M., et al. (2022). Phase-separating RNA-binding proteins form heterogeneous distributions of clusters in subsaturated solutions. Proc. Natl. Acad. Sci. USA 119, e2202222119. https://doi.org/10.1073/pnas.2202222119.
- 14. Ditlev, J.A., Case, L.B., and Rosen, M.K. (2018). Who's In and Who's Out-Compositional Control of Biomolecular Condensates. J. Mol. Biol. 430, 4666-4684. https://doi.org/10.1016/j.jmb.2018.08.003.
- 15. Hubatsch, L., Jawerth, L.M., Love, C., Bauermann, J., Tang, T.D., Bo, S., Hyman, A.A., and Weber, C.A. (2021). Quantitative theory for the diffusive dynamics of liquid condensates. Elife 10, e68620. https://doi.org/10.7554/ eLife.68620.
- 16. Taylor, N.O., Wei, M.-T., Stone, H.A., and Brangwynne, C.P. (2019). Quantifying Dynamics in Phase-Separated Condensates Using Fluorescence Recovery after Photobleaching. Biophys. J. 117, 1285–1300. https://doi. org/10.1016/j.bpj.2019.08.030.
- 17. Collins, M., Tomares, D.T., Schrader, J.M., and Childers, W.S. (2023). RNase E Biomolecular Condensates Stimulate PNPase Activity. Sci. Rep. 13, 12937. https://doi.org/10.1038/s41598-023-39565-w.
- 18. Peeples, W., and Rosen, M.K. (2021). Mechanistic dissection of increased enzymatic rate in a phase-separated compartment. Nat. Chem. Biol. 17, 693-702. https://doi.org/10.1038/s41589-021-00801-x.
- 19. Tibble, R.W., Depaix, A., Kowalska, J., Jemielity, J., and Gross, J.D. (2021). Biomolecular condensates amplify mRNA decapping by biasing enzyme conformation. Nat. Chem. Biol. 17, 615-623. https://doi.org/10. 1038/s41589-021-00774-x.
- 20. Moon, S.L., Morisaki, T., Khong, A., Lyon, K., Parker, R., and Stasevich, T.J. (2019). Multicolour single-molecule tracking of mRNA interactions with RNP granules. Nat. Cell Biol. 21, 162-168. https://doi.org/10.1038/ s41556-018-0263-4.
- 21. Pitchiaya, S., Mourao, M.D.A., Jalihal, A.P., Xiao, L., Jiang, X., Chinnaiyan, A.M., Schnell, S., and Walter, N.G. (2019). Dynamic Recruitment of Single RNAs to Processing Bodies Depends on RNA Functionality. Mol. Cell 74, 521-533.e6. https://doi.org/10.1016/j.molcel.2019.03.001.

- 22. Hubstenberger, A., Courel, M., Bénard, M., Souquere, S., Ernoult-Lange, M., Chouaib, R., Yi, Z., Morlot, J.-B., Munier, A., Fradet, M., et al. (2017). P-Body Purification Reveals the Condensation of Repressed mRNA Regulons. Mol. Cell 68, 144-157.e5. https://doi.org/10.1016/j.molcel.2017. 09.003.
- 23. Jain, S., Wheeler, J.R., Walters, R.W., Agrawal, A., Barsic, A., and Parker, R. (2016). ATPase-Modulated Stress Granules Contain a Diverse Proteome and Substructure. Cell 164, 487-498. https://doi.org/10.1016/j.cell.
- 24. Khong, A., Matheny, T., Jain, S., Mitchell, S.F., Wheeler, J.R., and Parker, R. (2017). The Stress Granule Transcriptome Reveals Principles of mRNA Accumulation in Stress Granules. Mol. Cell 68, 808-820.e5. https://doi. org/10.1016/j.molcel.2017.10.015.
- 25. Markmiller, S., Soltanieh, S., Server, K.L., Mak, R., Jin, W., Fang, M.Y., Luo, E.-C., Krach, F., Yang, D., Sen, A., et al. (2018). Context-Dependent and Disease-Specific Diversity in Protein Interactions within Stress Granules. Cell 172, 590-604.e13. https://doi.org/10.1016/j.cell.2017.12.032.
- 26. Youn, J.-Y., Dunham, W.H., Hong, S.J., Knight, J.D.R., Bashkurov, M., Chen, G.I., Bagci, H., Rathod, B., MacLeod, G., Eng, S.W.M., et al. (2018). High-Density Proximity Mapping Reveals the Subcellular Organization of mRNA-Associated Granules and Bodies. Mol. Cell 69, 517-532.e11. https://doi.org/10.1016/j.molcel.2017.12.020.
- 27. Xing, W., Muhlrad, D., Parker, R., and Rosen, M.K. (2020). A quantitative inventory of yeast P body proteins reveals principles of composition and specificity. Elife 9, e56525. https://doi.org/10.7554/eLife.56525.
- 28. Currie, S.L., Xing, W., Muhlrad, D., Decker, C.J., Parker, R., and Rosen, M.K. (2023). Quantitative Reconstitution of Yeast RNA Processing Bodies. Proc. Natl. Acad. Sci. USA 120, e2214064120. https://doi.org/10.1073/ pnas.2214064120.
- 29. Al-Husini, N., Tomares, D.T., Pfaffenberger, Z.J., Muthunayake, N.S., Samad, M.A., Zuo, T., Bitar, O., Aretakis, J.R., Bharmal, M.-H.M., Gega, A., et al. (2020). BR-Bodies Provide Selectively Permeable Condensates that Stimulate mRNA Decay and Prevent Release of Decay Intermediates. Mol. Cell 78, 670-682.e8. https://doi.org/10.1016/j.molcel.2020.04.001.
- 30. Muthunayake, N.S., Al-Husini, N., and Schrader, J.M. (2020). Differential Centrifugation to Enrich Bacterial Ribonucleoprotein Bodies (BR bodies) from Caulobacter crescentus. STAR Protoc. 1, 100205. https://doi.org/ 10.1016/j.xpro.2020.100205.
- 31. Hardwick, S.W., Chan, V.S.Y., Broadhurst, R.W., and Luisi, B.F. (2011). An RNA degradosome assembly in Caulobacter crescentus. Nucleic Acids Res. 39, 1449-1459. https://doi.org/10.1093/nar/gkq928.
- 32. Canestrari, J.G., Lasek-Nesselquist, E., Upadhyay, A., Rofaeil, M., Champion, M.M., Wade, J.T., Derbyshire, K.M., and Gray, T.A. (2020). Polycysteine-encoding leaderless short ORFs function as cysteine-responsive attenuators of operonic gene expression in mycobacteria. Mol. Microbiol. 114, 93-108. https://doi.org/10.1111/mmi.14498.
- 33. Mousseau, C.B., Pierre, C.A., Hu, D.D., and Champion, M.M. (2022). Miniprep assisted proteomics (MAP) for rapid proteomics sample preparation. Anal. Methods 10. https://doi.org/10.1039/D2AY01549H.
- 34. Voss, J.E., Luisi, B.F., and Hardwick, S.W. (2014). Molecular recognition of RhIB and RNase D in the Caulobacter crescentus RNA degradosome. Nucleic Acids Res. 42, 13294-13305. https://doi.org/10.1093/nar/gku1134.
- 35. Aguirre, A.A., Vicente, A.M., Hardwick, S.W., Alvelos, D.M., Mazzon, R.R., Luisi, B.F., and Marques, M.V. (2017). Association of the Cold Shock DEAD-Box RNA Helicase RhIE to the RNA Degradosome in Caulobacter crescentus. J. Bacteriol. 199, 001355-17-e217. https://doi.org/10.1128/ JB.00135-17.
- 36. Holmes, J.A., Follett, S.E., Wang, H., Meadows, C.P., Varga, K., and Bowman, G.R. (2016). Caulobacter PopZ forms an intrinsically disordered hub in organizing bacterial cell poles. Proc. Natl. Acad. Sci. USA 113, 12490-12495. https://doi.org/10.1073/pnas.1602380113.
- 37. Sherman, B.T., Hao, M., Qiu, J., Jiao, X., Baseler, M.W., Lane, H.C., Imamichi, T., and Chang, W. (2022). DAVID: a web server for functional





- enrichment analysis and functional annotation of gene lists (2021 update). Nucleic Acids Res. 50, W216-W221. https://doi.org/10.1093/nar/ akac194.
- 38. Ghosh, A., Bharmal, M.-H.M., Ghaleb, A.M., Nandana, V., and Schrader, J.M. (2023). Initiator AUGs Are Discriminated from Elongator AUGs Predominantly through mRNA Accessibility in C. crescentus. J. Bacteriol. 205, e0042022-e00422. https://doi.org/10.1128/jb.00420-22.
- 39. Russell, J.H., and Keiler, K.C. (2009). Subcellular localization of a bacterial regulatory RNA. Proc. Natl. Acad. Sci. USA 106, 16405-16409. https://doi. org/10.1073/pnas.0904904106.
- 40. Ducret, A., Quardokus, E.M., and Brun, Y.V. (2016). MicrobeJ, a tool for high throughput bacterial cell detection and quantitative analysis. Nat. Microbiol. 1, 16077-7. https://doi.org/10.1038/nmicrobiol.2016.77.
- 41. Aretakis, J.R., Gega, A., and Schrader, J.M. (2019). Absolute Measurements of mRNA Translation in Caulobacter crescentus Reveal Important Fitness Costs of Vitamin B12 Scavenging. mSystems 4, 001700-19e219. https://doi.org/10.1128/mSystems.00170-19.
- 42. Hondele, M., Sachdev, R., Heinrich, S., Wang, J., Vallotton, P., Fontoura, B.M.A., and Weis, K. (2019). DEAD-box ATPases are global regulators of phase-separated organelles. Nature 573, 144-148. https://doi.org/10. 1038/s41586-019-1502-y.
- 43. Beaufay, F., Amemiya, H.M., Guan, J., Basalla, J., Meinen, B.A., Chen, Z., Mitra, R., Bardwell, J.C.A., Biteen, J.S., Vecchiarelli, A.G., et al. (2021). Polyphosphate drives bacterial heterochromatin formation. Sci. Adv. 7, eabk0233. https://doi.org/10.1126/sciadv.abk0233.
- 44. Romero, P., Obradovic, Z., Kissinger, C., Villafranca, J.E., and Dunker, A.K. (1997). Identifying disordered regions in proteins from amino acid sequence. In Proceedings of International Conference on Neural Networks (ICNN'97), pp. 90-95. https://doi.org/10.1109/ICNN.1997.611643
- 45. Vernon, R.M., Chong, P.A., Tsang, B., Kim, T.H., Bah, A., Farber, P., Lin, H., and Forman-Kay, J.D. (2018). Pi-Pi contacts are an overlooked protein feature relevant to phase separation. Elife 7, e31486. https://doi.org/10. 7554/eLife.31486.
- 46. Bolognesi, B., Lorenzo Gotor, N., Dhar, R., Cirillo, D., Baldrighi, M., Tartaglia, G.G., and Lehner, B. (2016). A Concentration-Dependent Liquid Phase Separation Can Cause Toxicity upon Increased Protein Expression. Cell Rep. 16, 222-231. https://doi.org/10.1016/j.celrep.2016.05.076.
- 47. Saar, K.L., Morgunov, A.S., Qi, R., Arter, W.E., Krainer, G., Lee, A.A., and Knowles, T.P.J. (2021). Learning the molecular grammar of protein condensates from sequence determinants and embeddings. Proc. Natl. Acad. Sci. USA 118, e2019053118. https://doi.org/10.1073/pnas. 2019053118.
- 48. Postma, M., and Goedhart, J. (2019). PlotsOfData A web app for visualizing data together with their summaries. PLoS Biol. 17, e3000202. https:// doi.org/10.1371/journal.pbjo.3000202.
- 49. Karimova, G., Pidoux, J., Ullmann, A., and Ladant, D. (1998). A bacterial two-hybrid system based on a reconstituted signal transduction pathway. Proc. Natl. Acad. Sci. USA 95, 5752-5756. https://doi.org/10.1073/pnas.
- 50. Thanbichler, M., Iniesta, A.A., and Shapiro, L. (2007). A comprehensive set of plasmids for vanillate- and xylose-inducible gene expression in Caulobacter crescentus. Nucleic Acids Res. 35, e137. https://doi.org/10.1093/
- 51. Krypotou, E., Townsend, G.E., Gao, X., Tachiyama, S., Liu, J., Pokorzynski, N.D., Goodman, A.L., and Groisman, E.A. (2023). Bacteria require phase separation for fitness in the mammalian gut. Science 379, 1149-1156. https://doi.org/10.1126/science.abn7229.
- 52. Tauber, D., Tauber, G., Khong, A., Van Treeck, B., Pelletier, J., and Parker, R. (2020). Modulation of RNA Condensation by the DEAD-Box Protein elF4A. Cell 180, 411-426.e16. https://doi.org/10.1016/j.cell.2019.12.031.
- 53. Assis, N.G., Ribeiro, R.A., da Silva, L.G., Vicente, A.M., Hug, I., and Marques, M.V. (2019). Identification of Hfq-binding RNAs in Caulobacter cres-

- centus. RNA Biol. 16, 719-726. https://doi.org/10.1080/15476286.2019. 1503001
- 54. Møller, T., Franch, T., Højrup, P., Keene, D.R., Bächinger, H.P., Brennan, R.G., and Valentin-Hansen, P. (2002). Hfq: A Bacterial Sm-like Protein that Mediates RNA-RNA Interaction. Mol. Cell 9, 23-30. https://doi.org/ 10.1016/S1097-2765(01)00436-1.
- 55. Updegrove, T.B., Zhang, A., and Storz, G. (2016). Hfq: the flexible RNA matchmaker. Curr. Opin. Microbiol. 30, 133-138. https://doi.org/10. 1016/i.mib.2016.02.003.
- 56. Urban, J.H., and Vogel, J. (2008). Two Seemingly Homologous Noncoding RNAs Act Hierarchically to Activate glmS mRNA Translation. PLoS Biol. 6, e64. https://doi.org/10.1371/journal.pbio.0060064.
- 57. Vogel, J., and Luisi, B.F. (2011). Hfq and its constellation of RNA. Nat. Rev. Microbiol. 9, 578-589. https://doi.org/10.1038/nrmicro2615.
- 58. Ikeda, Y., Yagi, M., Morita, T., and Aiba, H. (2011). Hfq binding at RhIBrecognition region of RNase E is crucial for the rapid degradation of target mRNAs mediated by sRNAs in Escherichia coli. Mol. Microbiol. 79, 419-432. https://doi.org/10.1111/j.1365-2958.2010.07454.x.
- 59. Fei, J., Singh, D., Zhang, Q., Park, S., Balasubramanian, D., Golding, I., Vanderpool, C.K., and Ha, T. (2015). Determination of in vivo target search kinetics of regulatory noncoding RNA. Science 347, 1371-1374. https:// doi.org/10.1126/science.1258849.
- 60. Duval, M., Korepanov, A., Fuchsbauer, O., Fechter, P., Haller, A., Fabbretti, A., Choulier, L., Micura, R., Klaholz, B.P., Romby, P., et al. (2013). Escherichia coli Ribosomal Protein S1 Unfolds Structured mRNAs Onto the Ribosome for Active Translation Initiation. PLoS Biol. 11, e1001731. https://doi.org/10.1371/journal.pbio.1001731.
- 61. Delvillani, F., Papiani, G., Dehò, G., and Briani, F. (2011). S1 ribosomal protein and the interplay between translation and mRNA decay. Nucleic Acids Res. 39, 7702-7715. https://doi.org/10.1093/nar/gkr417.
- 62. Robledo, M., García-Tomsig, N.I., Matia-González, A.M., García-Rodríguez, F.M., and Jiménez-Zurdo, J.I. (2021). Synthetase of the methyl donor S-adenosylmethionine from nitrogen-fixing α-rhizobia can bind functionally diverse RNA species. RNA Biol. 18, 1111-1123. https://doi. org/10.1080/15476286.2020.1829365.
- 63. Britos, L., Abeliuk, E., Taverner, T., Lipton, M., McAdams, H., and Shapiro, L. (2011). Regulatory Response to Carbon Starvation in Caulobacter crescentus. PLoS One 6, e18179. https://doi.org/10.1371/journal.pone. 0018179.
- 64. Cabrera, J.E., Cagliero, C., Quan, S., Squires, C.L., and Jin, D.J. (2009). Active Transcription of rRNA Operons Condenses the Nucleoid in Escherichia coli: Examining the Effect of Transcription on Nucleoid Structure in the Absence of Transertion. J. Bacteriol. 191, 4180-4185. https://doi. ora/10.1128/JB.01707-08.
- 65. Queiroz, R.M.L., Smith, T., Villanueva, E., Marti-Solano, M., Monti, M., Pizzinga, M., Mirea, D.-M., Ramakrishna, M., Harvey, R.F., Dezi, V., et al. (2019). Comprehensive identification of RNA-protein interactions in any organism using orthogonal organic phase separation (OOPS). Nat. Biotechnol. 37, 169-178. https://doi.org/10.1038/s41587-018-0001-2.
- 66. Shchepachev, V., Bresson, S., Spanos, C., Petfalski, E., Fischer, L., Rappsilber, J., and Tollervey, D. (2019). Defining the RNA interactome by total RNA-associated protein purification. Mol. Syst. Biol. 15, e8689. https:// doi.org/10.15252/msb.20188689.
- 67. Hentze, M.W., Castello, A., Schwarzl, T., and Preiss, T. (2018). A brave new world of RNA-binding proteins. Nat. Rev. Mol. Cell Biol. 19, 327-341. https://doi.org/10.1038/nrm.2017.130.
- 68. van Mierlo, G., Jansen, J.R.G., Wang, J., Poser, I., van Heeringen, S.J., and Vermeulen, M. (2021). Predicting protein condensate formation using machine learning. Cell Rep. 34, 108705. https://doi.org/10.1016/j.celrep. 2021.108705.
- 69. Riback, J.A., Katanski, C.D., Kear-Scott, J.L., Pilipenko, E.V., Rojek, A.E., Sosnick, T.R., and Drummond, D.A. (2017). Stress-Triggered Phase

Cell Reports Article



- Separation Is an Adaptive, Evolutionarily Tuned Response. Cell 168, 1028-1040.e19. https://doi.org/10.1016/j.cell.2017.02.027.
- 70. Rueden, C.T., Schindelin, J., Hiner, M.C., DeZonia, B.E., Walter, A.E., Arena, E.T., and Eliceiri, K.W. (2017). ImageJ2: ImageJ for the next generation of scientific image data. BMC Bioinformatics 18, 529. https://doi.org/ 10.1186/s12859-017-1934-z.
- 71. Evinger, M., and Agabian, N. (1977). Envelope-associated nucleoid from Caulobacter crescentus stalked and swarmer cells. J. Bacteriol. 132, 294-301. https://doi.org/10.1128/jb.132.1.294-301.1977.
- 72. Schrader, J.M., and Shapiro, L. (2015). Synchronization of Caulobacter Crescentus for Investigation of the Bacterial Cell Cycle. JoVEe52633. https://doi.org/10.3791/52633.
- 73. Cronin, R.M., Ferrell, M.J., Cahir, C.W., Champion, M.M., and Champion, P.A. (2022). Proteo-genetic analysis reveals clear hierarchy of ESX-1 secretion in Mycobacterium marinum. Proc. Natl. Acad. Sci. USA 119, e2123100119. https://doi.org/10.1073/pnas.2123100119.
- 74. Jing, B., Xu, D., Wang, X., and Zhu, Y. (2018). Multiresponsive, Critical Gel Behaviors of Polyzwitterion-Polyoxometalate Coacervate Complexes. Macromolecules 51, 9405-9411. https://doi.org/10.1021/acs.macromol. 8b01759.





STAR***METHODS**

KEY RESOURCES TABLE

REAGENT or RESOURCE	SOURCE	IDENTIFIER
Bacterial and virus strains		
Caulobacter crescentus NA1000	Lucy Shapiro, Stanford University School of Medicine	N/A
TOP10 E. coli	Thermofisher scientific	C404010
BL21(DE3) E. coli	NEB	C2527I
Chemicals, peptides, and recombinant protein	ns .	
рСр- Су5	Jena Bioscience	NU-1706-CY5
cy5-NHS ester	Lumiprobe	13020
PMSF (phenylmethylsulfonyl fluoride)	RPI	P20270-5G
Phusion DNA Polymease	Thermo Scientific	F-530L
EDTA-free protease	Rouch	11873580001
RNAprotect Bacterial Reagent	QIAGEN	76506
SYBR-Gold nucleic acid gel stain	Invitrogen	S11494
TRizol Reagent	Ambion	15596018
Vanillic acid	Fluka	94770-50G
Xylose	Sigma Aldrich	X1500-500G
RNase A	Sigma Aldrich	R-5503 500mg
Dextrin XPure Agarose Resin	UBPBio	P3080-50
See Table S6 for a list of recombinant	N/A	N/A
proteins used in this study		
Deposited data		
LC-MS data	MassIVE proteomics database https://massive.ucsd.edu/ProteoSAFe/dataset. jsp?task = 9e8f620d6d3a4b1b82b691b9c246b68f	accession number MSV000090894
Experimental models: Organisms/strains		
See Table S5 for a list of bacterial strains	N/A	N/A
Oligonucleotides		
See Table S3 for a list of oligonucleotides in this study.	N/A	N/A
Recombinant DNA		
See Table S4 for a list of recombinant plasmids used	N/A	N/A
Software and algorithms		
microbeJ	Ducret et al. ⁴⁰	https://www.microbej.com/
mageJ	Rueden et al. ⁷⁰	https://ImageJ.nih.gov/
PlotsOfData	Postma et al. ⁴⁸	https://huygens.science.uva.nl/ PlotsOfData/
Other		
Microscope	Nikon	Ni-E
CCD camera	CoolSnap	Муо
YFP filter cube	Chroma	96363
GFP filter cube	Chroma	96362
CFP filter cube	Chroma	96361
TX-Red filter cube	Chroma	96322
Microscope slide/white epoxy ink frosted end one side	Thermo SCIENTIFIC	3051

(Continued on next page)



Continued		
REAGENT or RESOURCE	SOURCE	IDENTIFIER
Microscope cover glass	Fisher brand	12-545-M
Confocal microscope	Zeiss	LSM 800
IX71 inverted epifluorescence microscope	Olympus	N/A

RESOURCE AVAILABILITY

Lead contact

Further information and requests for resources and reagents should be directed to and will be fulfilled by the Lead Contact: Jared Schrader, Schrader@wayne.edu.

Materials availability

All strains and plasmids generated in this work will be made available upon request to the lead contact without restriction.

Data and code availability

- Proteomics data are available on the MassIVE database with accession number (MassIVE: MSV000090894).
- This paper does not report original custom code.
- Any additional information required to reanalyze the data reported in this paper is available from the lead contact upon request.

EXPERIMENTAL MODEL AND STUDY PARTICIPANT DETAILS

Caulobacter crescentus

All Caulobacter crescentus strains used in this study were derived from the wild-type strain NA1000⁷¹ and were grown at 28°C in peptone-yeast extract (PYE) medium or M2 minimal medium supplemented with 0.2% D-glucose (M2G).⁷² When appropriate, the indicated concentration of vanillate (0.5 mM), xylose (0.2%), gentamycin (Gent) (0.5 mg/mL), kanamycin (Kan) (5 mg/mL), spectinomycin (Spec) (25 mg/mL), and/or streptomycin (Strp) (5 mg/mL) was added. Strains were analyzed at mid-exponential phase of growth (OD 0.3-0.6). Optical density was measured at 600 nm in a cuvette using a Nanodrop 2000C spectrophotometer.

METHOD DETAILS

Plasmid construction

Protein expression plasmids construction

NudC-pET28a-2 plasmid was generated by subcloning from pVNudC-YFPC-2 into pET28a-2 plasmid. First, both pVNudC-YFPC-2 and pET28a-2 were cut with Nde1/EcoRI enzymes. Next, the digested fragments were gel purified, then ligated using T4 DNA ligase enzyme. The ligation was transformed into chemically competent E. coli cells and selected on LB-Kan plates. The resulting kanR colonies were then screened by PCR for the insert and verified by sanger sequencing (genewiz).

RppH-pET28a-2 plasmid was generated by subcloning from pVRppH-YFPC-2 into pET28a-2 plasmid. First, both pVRppH-YFPC-2 and pET28a-2 were cut with Nde1/EcoRl enzymes. Next, the digested fragments were gel purified, then ligated using T4 DNA ligase enzyme. The ligation was transformed into chemically competent E. coli cells and selected on LB-Kan plates. The resulting kanR colonies were then screened by PCR for the insert and verified by sanger sequencing (genewiz).

Rho-pET28a-2 plasmid was generated by subcloning from pVRhO-YFPC-2 into pET28a-2 plasmid. First, both pVRhO-YFPC-2 and pET28a-2 were cut with Nde1/EcoRI enzymes. Next, the digested fragments were gel purified, then ligated using T4 DNA ligase enzyme. The ligation was transformed into chemically competent E. coli cells and selected on LB-Kan plates. The resulting kanR colonies were then screened by PCR for the insert and verified by sanger sequencing (genewiz).

MetK-pET28a-2 plasmid was generated by subcloning from pVMetK-YFPC-2 into pET28a-2 plasmid. First, both pVMetK-YFPC-2 and pET28a-2 were cut with Nde1/EcoRI enzymes. Next, the digested fragments were gel purified, then ligated using T4 DNA ligase enzyme. The ligation was transformed into chemically competent E. coli cells and selected on LB-Kan plates. The resulting kanR colonies were then screened by PCR for the insert and verified by sanger sequencing (genewiz).

FabG-pET28a-2 plasmid was generated by subcloning from pVFabG-YFPC-2 into pET28a-2 plasmid. First, both pVFabG-YFPC-2 and pET28a-2 were cut with Nde1/EcoRI enzymes. Next, the digested fragments were gel purified, then ligated using T4 DNA ligase enzyme. The ligation was transformed into chemically competent E. coli cells and selected on LB-Kan plates. The resulting kanR colonies were then screened by PCR for the insert and verified by sanger sequencing (genewiz).

HFQ-pET-28a(+) plasmid was generated by GenScript as a gblock fragment. The gbock fragment was cloned into pET-28a vector by GenScript.





Hfq qblock

GGCCGCAAGCTTGTCGACGGAGCTCGAATTCgcgtcgtcggcgtcggcgtcggctcatagagctgaacgggttgagccggcatgatggtggaaatggcgtg cttgtagaccagttgcgactggcgtcgcgacgcagcaggacgcagaaattgtcgaaccagctgaccacgccctgcagcttgacgccattgacgacgaagaagatggtgagcggc gtcttcgacttgcgaacgctgttcaggaaggtgtcctgaagattttgcttcttttcggcggaCATATGGCTGCCGCGCGCACCAGGCCGCTG

The protein expression genes in pVN001, pVN004, pVN028, pVN030 plasmids were amplified from C. crescentus genomic DNA using VN003F & VN003R, VN001F & VN002R, VN004F & VN034R, VN035F & VN036R oligos respectively and cloned separately into pET-MBP-TEV-His vector using Ssp1 and HindIII restriction sites. The genes in pVN008, pVN024, pVN027, pVN032, pVN034, pVN035, pVN045 plasmids were amplified from C. crescentus genomic DNA using VN004F & VN004R, VN019F & VN020R, VN026F & VN027R, VN037F & VN037R, VN039F & VN039R, VN040F & VN040R, VN019F & VN021R, VN062F & VN063R oligos respectively and cloned separately into pET-MBP-TEV-His vector using Ssp1 and HindIII restriction sites.

pMJC0100 plasmid was generated by amplifying the C. crescentus aconitase gene using primers MJC229 and MJC230 and inserted into pTEV5 using Gibson assembly. The Gibson reaction was transformed into chemically competent E. coli cells and selected on LB-Amp plates. The resulting ampR colonies were then screened by PCR for the insert and verified by sanger sequencing.

- 1. MJC229 CCAACTAGTGAAAACCTGTATTTTCAGGGCGCTATGGCGTCTGTGGACAGCCT.
- 2. MJC230 AGAATTCCATGGCCATATGGCTTTAGTCGGCCTTGGCCAGGTTCCGCAGC.

Caulobacter plasmid construction

All Caulobacter crescentus gene inserts were amplified by PCR from the NA1000 genome. PAPI-YFP fusion was generated by cloning the Papl gene (CCNA_00413) lacking a stop codon in frame with YFP in the pVYFPC-2 plasmid.⁵⁰ First, the Papl gene was amplified by PCR from the NA1000 genome using the following DNA primers:

- (1) F_00413 cgaggaaacgcatatgagcagtgaaatgatcggcaacgcg
- (2) R_00413 cgttcgaattcgcgtagaccatgccctgggcgacg

Next, the resulting PCR product was digested with Ndel and EcoRI enzymes, gel purified, then ligated to Ndel/EcoRI cut pVYFPC-2 plasmid using T4 DNA ligase enzyme. The ligation was transformed into chemically competent E. coli cells and selected on LB-Kan plates. The resulting kanR colonies were then screened by PCR for the insert and verified by sanger sequencing (genewiz). RhIE-YFP fusion was generated by cloning the RhIE gene (CCNA_00878) lacking a stop codon in frame with YFP in the pVYFPC-2 plasmid.⁵⁰ First, the RhIE gene was amplified by PCR from the NA1000 genome using the following DNA primers:

- (1) F_00878 cgatgcgaggaaacgcatatgactcaattttccgaccttggcct
- (2) R_00878 cgttcgaattcgcgtcgataggcgaccagcgc

Next, the resulting PCR product was digested with Ndel and EcoRI enzymes, gel purified, then ligated to Ndel/EcoRI cut pVYFPC-2 plasmid using T4 DNA ligase enzyme. The ligation was transformed into chemically competent E. coli cells and selected on LB-Kan plates. The resulting kanR colonies were then screened by PCR for the insert and verified by sanger sequencing (genewiz). Rho-YFP fusion was generated by cloning the Rho gene (CCNA_03876) lacking a stop codon in frame with YFP in the pVYFPC-2 plasmid.⁵⁰ First, the Rho gene was amplified by PCR from the NA1000 genome using the following DNA primers:

- (1) F_03876 cgaggaaacgcatatgaccgaagacaccgaaaaccagg
- (2) R_03876 cgttcgaattcgcggtgttcatcgactggaagaagtc

Next, the resulting PCR product was digested with Ndel and EcoRI enzymes, gel purified, then ligated to Ndel/EcoRI cut pVYFPC-2 plasmid using T4 DNA ligase enzyme. The ligation was transformed into chemically competent E. coli cells and selected on LB-Kan plates. The resulting kanR colonies were then screened by PCR for the insert and verified by sanger sequencing (genewiz). RppH-YFP fusion was generated by cloning the RppH gene (CCNA_03553) lacking a stop codon in frame with YFP in the pVYFPC-2 plasmid.⁵⁰ First, the RppH gene was amplified by PCR from the NA1000 genome using the following DNA primers:

- (1) F_03553 cgaggaaacgcatatgactgagctggaccatcctcaacatcg
- (2) R_03553 cgttcgaattcgcgttctcccctcgcggcg

Next, the resulting PCR product was digested with Ndel and EcoRI enzymes, gel purified, then ligated to Ndel/EcoRI cut pVYFPC-2 plasmid using T4 DNA ligase enzyme. The ligation was transformed into chemically competent E. coli cells and selected on LB-Kan plates. The resulting kanR colonies were then screened by PCR for the insert and verified by sanger sequencing (genewiz). NudC-YFP fusion was generated by cloning the NudC gene (CCNA_00267) lacking a stop codon in frame with YFP in the pVYFPC-2 plasmid.⁵⁰ First, the NudC gene was amplified by PCR from the NA1000 genome using the following DNA primers:

- (1) F_00267 gcgaggaaacgcatatgcctctttcgatcatcaccaacacc
- (2) R_00267 cgttcgaattcgccgcctcttcggcccaggc

Cell ReportsArticle



Next, the resulting PCR product was digested with Ndel and EcoRl enzymes, gel purified, then ligated to Ndel/EcoRl cut pVYFPC-2 plasmid using T4 DNA ligase enzyme. The ligation was transformed into chemically competent E. coli cells and selected on LB-Kan plates. The resulting kanR colonies were then screened by PCR for the insert and verified by sanger sequencing (genewiz). PNP-YFP fusion was generated by cloning the PNPase gene (CCNA_00033) lacking a stop codon in frame with YFP in the pVYFPC-2 plasmid. ⁵⁰ First, the PNPase gene was amplified by PCR from the NA1000 genome using the following DNA primers:

- (1) F_00033 cgatgcgaggaaacgcatatgttcgatatcaaacgcaagacgatcgagtggg
- (2) R_00033 cgttcgaattcgccgcctcttcggccgccgc

Next, the resulting PCR product was digested with Ndel and EcoRI enzymes, gel purified, then ligated to Ndel/EcoRI cut pVYFPC-2 plasmid using T4 DNA ligase enzyme. The ligation was transformed into chemically competent E. coli cells and selected on LB-Kan plates. The resulting kanR colonies were then screened by PCR for the insert and verified by sanger sequencing (genewiz). RNaseD1-YFP fusion was generated by cloning the RNaseD1 gene (CCNA_01776) lacking a stop codon in frame with YFP in the pVYFPC-2 plasmid.⁵⁰ First, the RNaseD1 gene was amplified by PCR from the NA1000 genome using the following DNA primers:

- (1) F_01776 cgaggaaacgcatatgaagctgatcaccaccaccacc
- (2) R_01776 cgtaacgttcgaattcgcatcgttcttgggggcgcg

Next, the resulting PCR product was digested with Ndel and EcoRI enzymes, gel purified, then ligated to Ndel/EcoRI cut pVYFPC-2 plasmid using T4 DNA ligase enzyme. The ligation was transformed into chemically competent E. coli cells and selected on LB-Kan plates. The resulting kanR colonies were then screened by PCR for the insert and verified by sanger sequencing (genewiz). RNaseD2-YFP fusion was generated by cloning the RNaseD2 gene (CCNA_03717) lacking a stop codon in frame with YFP in the pVYFPC-2 plasmid. First, the RNaseD2 gene was amplified by PCR from the NA1000 genome using the following DNA primers:

- (1) F_03717 gcgaggaaacgcatatggccaatttcgttcacgagggcg
- (2) R_03717 cgttcgaattcgcgctgtgggcgaagatgtccatctcc

Next, the resulting PCR product was digested with Ndel and EcoRI enzymes, gel purified, then ligated to Ndel/EcoRI cut pVYFPC-2 plasmid using T4 DNA ligase enzyme. The ligation was transformed into chemically competent E. coli cells and selected on LB-Kan plates. The resulting kanR colonies were then screened by PCR for the insert and verified by sanger sequencing (genewiz). RhIB-YFP fusion was generated by cloning the RhIB gene (CCNA_01923) lacking a stop codon in frame with YFP in the pVYFPC-2 plasmid.⁵⁰ First, the RhIB gene was amplified by PCR from the NA1000 genome using the following DNA primers:

- (1) F_01923 acgatgcgaggaaacgcatatgactgaattcaccgacctagggctatcg
- (2) R_01923 atcttaaggtacccttcgcgccgcgcggcgg

Next, the resulting PCR product was digested with Ndel and EcoRl enzymes, gel purified, then ligated to Ndel/EcoRl cut pVYFPC-2 plasmid using T4 DNA ligase enzyme. The ligation was transformed into chemically competent E. coli cells and selected on LB-Kan plates. The resulting kanR colonies were then screened by PCR for the insert and verified by sanger sequencing (genewiz). AconA-YFP fusion was generated by cloning the Aconitase gene (CCNA_03781) lacking a stop codon in frame with YFP in the pVYFPC-2 plasmid.⁵⁰ First, the Aconitase gene was amplified by PCR from the NA1000 genome using the following DNA primers:

- (1) F_03781 cgaggaaacgcatatggcgtctgtggacagc
- (2) R_03781 cgagatcttaaggtaccgtcggccttggccaggttc

Next, the resulting PCR product was digested with Ndel and EcoRI enzymes, gel purified, then ligated to Ndel/EcoRI cut pVYFPC-2 plasmid using T4 DNA ligase enzyme. The ligation was transformed into chemically competent E. coli cells and selected on LB-Kan plates. The resulting kanR colonies were then screened by PCR for the insert and verified by sanger sequencing (genewiz). RNaseJ-YFP fusion was generated by cloning the RNaseJ gene (CCNA_02012) lacking a stop codon in frame with YFP in the pVYFPC-2 plasmid. First, the RNaseJ gene was amplified by PCR from the NA1000 genome using the following DNA primers:

- (1) F_02012 tgcgaggaaacgcatatgaaaaagtccaagaacgacgag
- (2) R_02012 aacgttcgaattcgcaatgcgaagaaccgtgg

Next, the resulting PCR product was digested with Ndel and EcoRI enzymes, gel purified, then ligated to Ndel/EcoRI cut pVYFPC-2 plasmid using T4 DNA ligase enzyme. The ligation was transformed into chemically competent E. coli cells and selected on LB-Kan plates. The resulting kanR colonies were then screened by PCR for the insert and verified by sanger sequencing (genewiz). RNaseHI-YFP fusion was generated by cloning the RNaseHI gene (CCNA_03476) lacking a stop codon in frame with YFP in the pVYFPC-2 plasmid.⁵⁰ First, the RNaseHI gene was amplified by PCR from the NA1000 genome using the following DNA primers:

- (1) F_03476 cgaggaaacgcatatgacgccgaaggtcacgatctataccg
- (2) R_03476 cgtaacgttcgaattcgcgatgacgcgcggattgg





Next, the resulting PCR product was digested with Ndel and EcoRI enzymes, gel purified, then ligated to Ndel/EcoRI cut pVYFPC-2 plasmid using T4 DNA ligase enzyme. The ligation was transformed into chemically competent E. coli cells and selected on LB-Kan plates. The resulting kanR colonies were then screened by PCR for the insert and verified by sanger sequencing (genewiz). RNaseHII-YFP fusion was generated by cloning the RNaseHII gene (CCNA_00383) lacking a stop codon in frame with YFP in the pVYFPC-2 plasmid. First, the RNaseHII gene was amplified by PCR from the NA1000 genome using the following DNA primers:

- (1) F 00383 cgaggaaacgcatatgccgccggacccgac
- (2) R_00383 gcgtaacgttcgaattcgcaaggtctagctcgccgttgacc

Next, the resulting PCR product was digested with Ndel and EcoRI enzymes, gel purified, then ligated to Ndel/EcoRI cut pVYFPC-2 plasmid using T4 DNA ligase enzyme. The ligation was transformed into chemically competent E. coli cells and selected on LB-Kan plates. The resulting kanR colonies were then screened by PCR for the insert and verified by sanger sequencing (genewiz). SmpB-YFP fusion was generated by cloning the SmpB gene (CCNA_01254) lacking a stop codon in frame with YFP in the pVYFPC-2 plasmid. First, the SmpB gene was amplified by PCR from the NA1000 genome using the following DNA primers:

- (1) F_01254 cgaggaaacgcatatgatgtccaagccgatcgcg
- (2) R_01254 cgtaacgttcgaattcgtcgccgcgatcgcccttc

Next, the resulting PCR product was digested with Ndel and EcoRl enzymes, gel purified, then ligated to Ndel/EcoRl cut pVYFPC-2 plasmid using T4 DNA ligase enzyme. The ligation was transformed into chemically competent E. coli cells and selected on LB-Kan plates. The resulting kanR colonies were then screened by PCR for the insert and verified by sanger sequencing (genewiz). RNaseL-YFP fusion was generated by cloning the RNaseL gene (CCNA_01143) lacking a stop codon in frame with YFP in the pVYFPC-2 plasmid. First, the RNaseL gene was amplified by PCR from the NA1000 genome using the following DNA primers:

- (1) F_01143 cgaggaaacgcatatgaaacgcctgatcgctctcaccg
- (2) R_01143 gcgtaacgttcgaattcgctttcttcttggcggcctgg

Next, the resulting PCR product was digested with Ndel and EcoRl enzymes, gel purified, then ligated to Ndel/EcoRl cut pVYFPC-2 plasmid using T4 DNA ligase enzyme. The ligation was transformed into chemically competent E. coli cells and selected on LB-Kan plates. The resulting kanR colonies were then screened by PCR for the insert and verified by sanger sequencing (genewiz). RNaseP-YFP fusion was generated by cloning the RNaseP gene (CCNA_00807) lacking a stop codon in frame with YFP in the pVYFPC-2 plasmid. ⁵⁰ First, the RNaseP gene was amplified by PCR from the NA1000 genome using the following DNA primers:

- (1) F_00807 cgaggaaacgcatatggctgaagcgccgcacacc
- (2) R_00807 cgtaacgttcgaattcgcaccggaaactgtgggatcggg

Next, the resulting PCR product was digested with Ndel and EcoRI enzymes, gel purified, then ligated to Ndel/EcoRI cut pVYFPC-2 plasmid using T4 DNA ligase enzyme. The ligation was transformed into chemically competent E. coli cells and selected on LB-Kan plates. The resulting kanR colonies were then screened by PCR for the insert and verified by sanger sequencing (genewiz). RNaseT2-YFP fusion was generated by cloning the RNaseT2 gene (CCNA_00030) lacking a stop codon in frame with YFP in the pVYFPC-2 plasmid.⁵⁰ First, the RNaseT2 gene was amplified by PCR from the NA1000 genome using the following DNA primers:

- (1) F_00030 gcgaggaaacgcatatgttggagtcgccgatgaagaccg
- (2) R_00030 cgtaacgttcgaattcgcctgctggcctggtgagg

Next, the resulting PCR product was digested with Ndel and EcoRI enzymes, gel purified, then ligated to Ndel/EcoRI cut pVYFPC-2 plasmid using T4 DNA ligase enzyme. The ligation was transformed into chemically competent E. coli cells and selected on LB-Kan plates. The resulting kanR colonies were then screened by PCR for the insert and verified by sanger sequencing (genewiz). RNaseIII-YFP fusion was generated by cloning the RNaseIII gene (CCNA_01630) lacking a stop codon in frame with YFP in the pVYFPC-2 plasmid. First, the RNaseIII gene was amplified by PCR from the NA1000 genome using the following DNA primers:

- (1) F_01630 cgaggaaacgcatatggatagacgggtcgccgcc
- (2) R_01630 cgtaacgttcgaattcgcgcccgccccttcacgc

Next, the resulting PCR product was digested with Ndel and EcoRI enzymes, gel purified, then ligated to Ndel/EcoRI cut pVYFPC-2 plasmid using T4 DNA ligase enzyme. The ligation was transformed into chemically competent E. coli cells and selected on LB-Kan plates. The resulting kanR colonies were then screened by PCR for the insert and verified by sanger sequencing (genewiz). RNaseL1-YFP fusion was generated by cloning the RNaseL1 gene (CCNA_02241) lacking a stop codon in frame with YFP in the pVYFPC-2 plasmid.⁵⁰ First, the RNaseL1 gene was amplified by PCR from the NA1000 genome using the following DNA primers:

- (1) F_02241 gcgaggaaacgcatatggtgtgcatgtcgaccgtcg
- (2) R_02241 cgtaacgttcgaattcgcgatgatctccaccaccgcg

Cell ReportsArticle



Next, the resulting PCR product was digested with Ndel and EcoRl enzymes, gel purified, then ligated to Ndel/EcoRl cut pVYFPC-2 plasmid using T4 DNA ligase enzyme. The ligation was transformed into chemically competent E. coli cells and selected on LB-Kan plates. The resulting kanR colonies were then screened by PCR for the insert and verified by sanger sequencing (genewiz). RNaseR-YFP fusion was generated by cloning the RNaseR gene (CCNA_02537) lacking a stop codon in frame with YFP in the pVYFPC-2 plasmid. First, the RNaseR gene was amplified by PCR from the NA1000 genome using the following DNA primers:

- (1) F_02537 cgaggaaacgcatatgatggccaaacttcgccccacc
- (2) R_02537 gtaacgttcgaattcccgccgcttcccacgccg

Next, the resulting PCR product was digested with Ndel and EcoRI enzymes, gel purified, then ligated to Ndel/EcoRI cut pVYFPC-2 plasmid using T4 DNA ligase enzyme. The ligation was transformed into chemically competent E. coli cells and selected on LB-Kan plates. The resulting kanR colonies were then screened by PCR for the insert and verified by sanger sequencing (genewiz). FabG-YFP fusion was generated by cloning the FabG gene (CCNA_00545) lacking a stop codon in frame with YFP in the pVYFPC-2 plasmid. First, the FabG gene was amplified by PCR from the NA1000 genome using the following DNA primers:

- (1) F_00545 cgaggaaacgcatatgacgagagttgcgttcgtgaccg
- (2) R_00545 cgttcgaattcgcggccatgtactggccacc

Next, the resulting PCR product was digested with Ndel and EcoRI enzymes, gel purified, then ligated to Ndel/EcoRI cut pVYFPC-2 plasmid using T4 DNA ligase enzyme. The ligation was transformed into chemically competent E. coli cells and selected on LB-Kan plates. The resulting kanR colonies were then screened by PCR for the insert and verified by sanger sequencing (genewiz). MetK-YFP fusion was generated by cloning the MetK gene (CCNA_00048) lacking a stop codon in frame with YFP in the pVYFPC-2 plasmid.⁵⁰ First, the MetK gene was amplified by PCR from the NA1000 genome using the following DNA primers:

- (1) F_00048 cgaggaaacgcatttgagccgttcgtcctacatcttcacc
- (2) R_00048 cgtaacgttcgaattcgccgctaggcccttcaggtcg

Next, the resulting PCR product was digested with Ndel and EcoRI enzymes, gel purified, then ligated to Ndel/EcoRI cut pVYFPC-2 plasmid using T4 DNA ligase enzyme. The ligation was transformed into chemically competent E. coli cells and selected on LB-Kan plates. The resulting kanR colonies were then screened by PCR for the insert and verified by sanger sequencing (genewiz). NusG-YFP fusion was generated by cloning the NusG gene (CCNA_03310) lacking a stop codon in frame with YFP in the pVYFPC-2 plasmid.⁵⁰ First, the NusG gene was amplified by PCR from the NA1000 genome using the following DNA primers:

- (1) F_03310 cgaggaaacgcatatgagcaccgagaccgcg
- (2) R_03310 cgtaacgttcgaattcgcggcgatcttttcgacctgattgtattcc

Next, the resulting PCR product was digested with Ndel and EcoRI enzymes, gel purified, then ligated to Ndel/EcoRI cut pVYFPC-2 plasmid using T4 DNA ligase enzyme. The ligation was transformed into chemically competent E. coli cells and selected on LB-Kan plates. The resulting kanR colonies were then screened by PCR for the insert and verified by sanger sequencing (genewiz). RHF-YFP fusion was generated by cloning the RHF gene (CCNA_03711) lacking a stop codon in frame with YFP in the pVYFPC-2 plasmid. First, the RHF gene was amplified by PCR from the NA1000 genome using the following DNA primers:

- (1) F_03711 tgcgaggaaacgcatatgcaagtccaagtctccggca
- (2) R_03711 taacgttcgaattcgcgctcgcggttgatccgt

Next, the resulting PCR product was digested with Ndel and EcoRI enzymes, gel purified, then ligated to Ndel/EcoRI cut pVYFPC-2 plasmid using T4 DNA ligase enzyme. The ligation was transformed into chemically competent E. coli cells and selected on LB-Kan plates. The resulting kanR colonies were then screened by PCR for the insert and verified by sanger sequencing (genewiz).

TyrRS-YFP fusion was generated by cloning the TyrRS gene (CCNA_01946) lacking a stop codon in frame with YFP in the pVYFPC-2 plasmid.⁵⁰ First, the TyrRS gene was amplified by PCR from the NA1000 genome using the following DNA primers:

- (1) F_01946 gcgaggaaacgcatatgaacccctcacacaccgacc
- (2) R_01946 cgtaacgttcgaattcgcaacaggcttcaccaacacg

Next, the resulting PCR product was digested with Ndel and EcoRI enzymes, gel purified, then ligated to Ndel/EcoRI cut pVYFPC-2 plasmid using T4 DNA ligase enzyme. The ligation was transformed into chemically competent E. coli cells and selected on LB-Kan plates. The resulting kanR colonies were then screened by PCR for the insert and verified by sanger sequencing (genewiz). HFQ-YFP fusion was generated by GenScript as a gblock fragment. The gbock fragment was cloned into pVYFPC-4 vector by GenScript.





Gblock fragment

cgccgaaccacgatgcgaggaaacgcatatgtccgccgaaaagaagcaaaatcttcaggacaccttcctgaacagcgttcgcaagtcgaagacgccgctcaccatcttcctcg tcaatggcgtcaagctgcagggcgtggtcagctggttcgacaatttctgcgtcctgctgcgtcgcgacggccagtcgcaactggtctacaagcacgccatttccaccatcatgcc ggeteaaccegtteagetetatgageegagegeegaegaegaegaegaattegaaegttaegegteaeeggteggee

pBX-RhIE-YFP-2 plasmid was generated by subcloning the RhIE-YFP fragment from pVRhIE-YFPC-2 into pBXMCS-2 plasmid.⁵⁰ First, pVRhIE-YFPC-2 was cut with Nde1 and Nhe1 enzymes and pBXMCS-2 was cut with Nde1 and Xba1 enzymes. Next, the digested fragments were gel purified, then ligated using T4 DNA ligase enzyme. The ligation was transformed into chemically competent E. coli cells and selected on LB-Kan plates. The resulting kanR colonies were then screened by PCR for the insert and verified by sanger sequencing (genewiz).

pBX-MetK-YFP-2 plasmid was generated by subcloning the MetK-YFP fragment from pVMetK-YFPC-2 into pBXMCS-2⁵⁰ plasmid. First, pVMetK-YFPC-2 was cut with Nde1 and Nhe1 enzymes and pBXMCS-2 was cut with Nde1 and Xba1 enzymes. Next, the digested fragments were gel purified, then ligated using T4 DNA ligase enzyme. The ligation was transformed into chemically competent E. coli cells and selected on LB-Kan plates. The resulting kanR colonies were then screened by PCR for the insert and verified by sanger sequencing (genewiz).

pBX-S1-2 plasmid was generated by cloning the Ribosomal Protein S1 gene (CCNA_03702) in the pBXMCS-2 plasmid.⁵⁰ First, the Ribosomal Protein S1 gene was amplified by PCR from the NA1000 genome using the following DNA primers:

- (1) IW002_22 RPS1_F_Nde1 ggagacgaccatatgatggctgacgatatgagcttca
- (2) IW003_22 RPS1_R_Xba1 ggccgctctagattagtccttggaggcccgctcgcg

Next, the resulting PCR product was digested with Ndel and Xba1 enzymes, gel purified, then ligated to Ndel/Xba1 cut pBXMCS-2 plasmid using T4 DNA ligase enzyme. The ligation was transformed into chemically competent E. coli cells and selected on LB-Kan plates. The resulting kanR colonies were then screened by PCR for the insert and verified by sanger seguencing (genewiz).

pBX-MetK-2 plasmid was generated from pBX-MetK-YFP-2 plasmid by the inverse PCR using the following primers.

- (1) IW007 22 metK F taagctagagcggcggcaccg
- (2) IW006_22 metK_R cgctaggcccttcaggtcgcccaccagat

First, the fragment was PCR amplified using the T4 PNK kinased oligos and using pBX-MetK-YFP-2 plasmid as a template. The PCR product was then DPNI treated to cut the template DNA using DPNI enzyme (Thermoscientific 10 U/µI). The DPNI treated sample was gel purified and self-ligated. The ligation was transformed into E. coli cells and selected on LB-kan plates. The resulting kan^H colonies were then screened by PCR for the insert and verified by sanger sequencing (genewiz).

Bacterial 2 hybrid plasmids

pVN054

RNase E fragment was amplified from Caulobacter genomic DNA using VN084F and VN085R oligonucleotides and cloned into pKNT25 plasmid using Xba1 and EcoR1 restriction sites.

MetK gene was amplified from Caulobacter genomic DNA using VN087F and VN088R oligonucleotides and cloned into pUT18 plasmid using Xba1 and Sac1 restriction sites.

pVN057

Aconitase gene was amplified from Caulobacter genomic DNA using VN090F and VN091R oligonucleotides and cloned into pUT18 plasmid using Xba1 and Kpn1 restriction sites.

pVN058

Ribosomal protein S1 gene was amplified from Caulobacter genomic DNA using VN096F and VN097R oligonucleotides and cloned into pUT18 plasmid using Xba1 and Sac1 restriction sites.

pKT25-Zip, pUT18C-Zip, pKNT25 and pUT18 plasmids were obtained from BACTH kit.

Strain construction

JS370 NA1000 vanApapI-YFP Kan^R. The purified pVPAPI-YFPC-2 plasmid was transformed into NA1000 cells via electroporation and plated on PYE-Kan plates. The resulting colonies were grown in the presence and absence of vanillate and verified by fluorescence microscopy and further verified by integration PCR.

JS371 NA1000 vanArhIE-YFP Kan^R. The purified pVRhIE-YFPC-2 plasmid was transformed into NA1000 cells via electroporation and plated on PYE-Kan plates. The resulting colonies were grown in the presence and absence of vanillate and verified by fluorescence microscopy and further verified by integration PCR.

JS372 NA1000 vanArho-YFP Kan^R. The purified pVRhO-YFPC-2 plasmid was transformed into NA1000 cells via electroporation and plated on PYE-Kan plates. The resulting colonies were grown in the presence and absence of vanillate and verified by fluorescence microscopy and further verified by integration PCR.

Cell ReportsArticle



JS375 NA1000 vanArppH-YFP Kan^R. The purified pVRppH-YFPC-2 plasmid was transformed into NA1000 cells via electroporation and plated on PYE-Kan plates. The resulting colonies were grown in the presence and absence of vanillate and verified by fluorescence microscopy and further verified by integration PCR.

JS382 NA 10000 vanAnudC-YFP Kan^R. The purified pVNudC-YFPC-2 plasmid was transformed into NA1000 cells via electroporation and plated on PYE-Kan plates. The resulting colonies were grown in the presence and absence of vanillate and verified by fluorescence microscopy and further verified by integration PCR.

JS384 NA 10000 vanApnp-YFP Kan^R. The purified pVPNP-YFPC-2 plasmid was transformed into NA1000 cells via electroporation and plated on PYE-Kan plates. The resulting colonies were grown in the presence and absence of vanillate and verified by fluorescence microscopy and further verified by integration PCR.

JS399 NA 10000 vanArhlB-YFP Kan^R. The purified pVRhlB-YFPC-2 plasmid was transformed into NA1000 cells via electroporation and plated on PYE-Kan plates. The resulting colonies were grown in the presence and absence of vanillate and verified by fluorescence microscopy and further verified by integration PCR.

JS410 NA 10000 vanAacnA-YFP Kan^R. The purified pVAconA-YFPC-2 plasmid was transformed into NA1000 cells via electroporation and plated on PYE-Kan plates. The resulting colonies were grown in the presence and absence of vanillate and verified by fluorescence microscopy and further verified by integration PCR.

JS431 NA 10000 vanArnaseJ-YFP Kan^R. The purified pVRNaseJ-YFPC-2 plasmid was transformed into NA1000 cells via electroporation and plated on PYE-Kan plates. The resulting colonies were grown in the presence and absence of vanillate and verified by fluorescence microscopy and further verified by integration PCR.

JS455 NA 10000 vanArnaseD1-YFP Kan^R. The purified pVRNaseD1-YFPC-2 plasmid was transformed into NA1000 cells via electroporation and plated on PYE-Kan plates. The resulting colonies were grown in the presence and absence of vanillate and verified by fluorescence microscopy and further verified by integration PCR.

JS481 NA 10000 vanArnaseHI-YFP Kan^R. The purified pVRNaseHI-YFPC-2 plasmid was transformed into NA1000 cells via electroporation and plated on PYE-Kan plates. The resulting colonies were grown in the presence and absence of vanillate and verified by fluorescence microscopy and further verified by integration PCR.

JS482 NA 10000 vanArnaseHII-YFP Kan^R. The purified pVRNaseHII-YFPC-2 plasmid was transformed into NA1000 cells via electroporation and plated on PYE-Kan plates. The resulting colonies were grown in the presence and absence of vanillate and verified by fluorescence microscopy and further verified by integration PCR.

JS483 NA 10000 vanAsmpb-YFP Kan^R. The purified pVSmpB-YFPC-2 plasmid was transformed into NA1000 cells via electroporation and plated on PYE-Kan plates. The resulting colonies were grown in the presence and absence of vanillate and verified by fluorescence microscopy and further verified by integration PCR.

JS506 NA1000 vanArnaseL-YFP Kan^R. The purified pVRNaseL-YFPC-2 plasmid was transformed into NA1000 cells via electroporation and plated on PYE-Kan plates. The resulting colonies were grown in the presence and absence of vanillate and verified by fluorescence microscopy and further verified by integration PCR.

JS508 NA1000 vanA rnaseP-YFP Kan^R. The purified pVRNaseP-YFPC-2 plasmid was transformed into NA1000 cells via electroporation and plated on PYE-Kan plates. The resulting colonies were grown in the presence and absence of vanillate and verified by fluorescence microscopy and further verified by integration PCR.

JS510 NA1000 vanArnaseT2-YFP Kan^R. The purified pVRNaseT2-YFPC-2 plasmid was transformed into NA1000 cells via electroporation and plated on PYE-Kan plates. The resulting colonies were grown in the presence and absence of vanillate and verified by fluorescence microscopy and further verified by integration PCR.

JS517 NA1000 vanA rnaseIII-YFP Kan^R. The purified pVRNaseIII-YFPC-2 plasmid was transformed into NA1000 cells via electroporation and plated on PYE-Kan plates. The resulting colonies were grown in the presence and absence of vanillate and verified by fluorescence microscopy and further verified by integration PCR.

JS543 NA1000 vanA rnaseL1-YFP Kan^R. The purified pVRNaseL1-YFPC-2 plasmid was transformed into NA1000 cells via electro-poration and plated on PYE-Kan plates. The resulting colonies were grown in the presence and absence of vanillate and verified by fluorescence microscopy and further verified by integration PCR.

JS560 NA1000 vanArnaseR-YFP Gent^R. The purified pVRNaseR-YFPC-4 plasmid was transformed into NA1000 cells via electroporation and plated on PYE-Gent plates. The resulting colonies were grown in the presence and absence of vanillate and verified by fluorescence microscopy and further verified by integration PCR.

JS678 NA1000 vanAfabG-YFP Kan^R. The purified pVFabG-YFPC-2 plasmid was transformed into NA1000 cells via electroporation and plated on PYE-Kan plates. The resulting colonies were grown in the presence and absence of vanillate and verified by fluorescence microscopy and further verified by integration PCR.

JS680 NA1000 vanAmetK-YFP Kan^R. The purified pVMetK-YFPC-2 plasmid was transformed into NA1000 cells via electroporation and plated on PYE-Kan plates. The resulting colonies were grown in the presence and absence of vanillate and verified by fluorescence microscopy and further verified by integration PCR.

JS688 NA1000 vanAnusG-YFPC Kan^R. The purified pVNusG-YFPC-2 plasmid was transformed into NA1000 cells via electroporation and plated on PYE-Kan plates. The resulting colonies were grown in the presence and absence of vanillate and verified by fluorescence microscopy and further verified by integration PCR.





JS690 NA1000 vanArhf-YFP Kan^R. The purified pV-RHF-YFPC-2 plasmid was transformed into NA1000 cells via electroporation and plated on PYE-Kan plates. The resulting colonies were grown in the presence and absence of vanillate and verified by fluorescence microscopy and further verified by integration PCR.

JS692 NA1000 vanAtyrRS-YFP Kan^R. The purified pVTyrRS-YFPC-2 plasmid was then transformed into NA1000 cells via electroporation and plated on PYE-Kan plates. The resulting colonies were grown in the presence and absence of vanillate and verified to be expressing the YFP fusion by fluorescence microscopy and further verified by integration PCR.

JS697 NA1000 vanAhfq-YFP Gent^R. The purified pVHFQ-YFPC-4 plasmid was transformed into NA1000 cells via electroporation and plated on PYE-Gent plates. The resulting colonies were grown in the presence and absence of vanillate and verified by fluorescence microscopy and further verified by integration PCR.

JS699 NA1000 vanAhfg-YFPC rnepXrnessrAC Gent^R Kan^R. This strain was generated by transducing JS697 cells with RNase E depletion phage lysate from JS84 strain. The transduced cells were plated in PYE-Gent-Kan-Xylose plates and the resultant colonies were grown in PYE-Gent-Kan media with and without xylose to verify the RNase E depletion phenotype.

JS694 NA1000 rnepXrnessrAC Gent^R. The plasmid pXMCS-4⁵⁰ containing last 500bp of RNase E gene was transformed into NA1000 cells via electroporation and the colonies were selected on PYE-Gent-Xylose plates. The integration of RNase E gene under the xylose inducible promoter was confirmed by growing the cells in the presence and absence of xylose.

JS701 NA1000 vanArhIE-YFPC rnepXrnessrAC Gent^R Kan^R. This strain was generated by transducing JS371 cells with RNase E depletion phage lysate from JS694 strain. The transduced cells were plated in PYE-Gent-Kan-Xylose plates and the resultant colonies were grown in PYE-Gent-Kan media with and without xylose to verify the RNase E depletion phenotype.

JS702 NA1000 vanArho-YFPC rnepXrnessrAC Gent^R Kan^R. This strain was generated by transducing JS372 cells with RNase E depletion phage lysate from JS694 strain. The transduced cells were plated in PYE-Gent-Kan-Xylose plates and the resultant colonies were grown in PYE-Gent-Kan media with and without xylose to verify the RNase E depletion phenotype.

JS706 NA1000 vanAmetK-YFPC mepXrnessrAC Gent^R Kan^R. This strain was generated by transducing JS680 cells with RNase E depletion phage lysate from JS694 strain. The transduced cells were plated in PYE-Gent-Kan-Xylose plates and the resultant colonies were grown in PYE-Gent-Kan media with and without xylose to verify the RNase E depletion phenotype.

JS709 NA1000 vanArnaseD1(CTD)-YFPC rnepXrnessrAC Gent^R Kan^R. This strain was generated by transducing JS397 cells with RNase E depletion phage lysate from JS694 strain. The transduced cells were plated in PYE-Gent-Kan-Xylose plates and the resultant colonies were grown in PYE-Gent-Kan media with and without xylose to verify the RNase E depletion phenotype.

JS451 NA1000 acnAacnA-Chy pBXMCS Spec^R Strp^R Kan^R. The strain was generated by electroporation of JS134⁴ with pBXMCS-2 plasmid. 50 The cells were plated on PYE-Spec-Strp-Kan plates. The resulting colonies were grown in the presence and absence of xylose and verified by fluorescence microscopy.

JS452 NA1000 acnAacnA-Chy rnepBXme-YFPC Spec^R Strp^R Kan^R. The strain was generated by electroporation of JS134⁴ with pBXRNE-YFP-2 plasmid.²⁹ The cells were plated on PYE-Spec-Strp-Kan plates. The resulting colonies were grown in the presence and absence of xylose and verified by fluorescence microscopy.

JS716 NA1000 acnAacnA-Chy rhlEpBXrhlE-YFPC Spec^R Strp^R Kan^R. The strain was generated by electroporation of JS134⁴ with pBX-RhIE-YFP-2 plasmid. The cells were plated on PYE-Spec-Strp-Kan plates. The resulting colonies were grown in the presence and absence of xylose and verified by fluorescence microscopy.

JS721 NA1000 acnAacnA-Chy RPS1pBXRPS1 Spec^R Strp^R Kan^R. The strain was generated by electroporation of JS134⁴ with pBX-S1-2 plasmid. The cells were plated on PYE-Spec-Strp-Kan plates. The resulting colonies were grown in the presence and absence of xylose and verified by fluorescence microscopy.

JS742 NA1000 acnAacnA-Chy metKpBXmetK Spec^R Strp^R Kan^R. The strain was generated by electroporation of JS134⁴ with pBX-MetK-2 plasmid. The cells were plated on PYE-Spec-Strp-Kan plates. The resulting colonies were grown in the presence and absence of xylose and verified by fluorescence microscopy.

JS563 NA1000 vanArhIE-YFP rnerne-CHYC Kan^R Gent^R. This strain was generated by transducing JS371 cells with pRNE-chy phage lysate from JS403 strain. The transduced cells were plated in PYE-Gent-Kan plates. The resulting colonies were grown in the presence and absence of vanillate and verified by fluorescence microscopy and further verified by integration PCR.

JS564 NA1000 vanArho-YFP rnerne-CHYC Kan^R Gent^R. This strain was generated by transducing JS372 cells with pRNE-chy phage lysate from JS403 strain. The transduced cells were plated in PYE-Gent-Kan plates. The resulting colonies were grown in the presence and absence of vanillate and verified by fluorescence microscopy and further verified by integration PCR.

JS570 NA1000 vanArnaseHI-YFP merne-CHYC Kan^R Gent^R. This strain was generated by transducing JS481 cells with pRNE-chy phage lysate from JS403 strain. The transduced cells were plated in PYE-Gent-Kan plates. The resulting colonies were grown in the presence and absence of vanillate and verified by fluorescence microscopy and further verified by integration PCR.

JS758 NA1000 vanArnaseD1-YFP merne-CHYC Kan^R Gent^R. This strain was generated by transducing JS455 cells with pRNE-chy phage lysate from JS403 strain. The transduced cells were plated in PYE-Gent-Kan plates. The resulting colonies were grown in the presence and absence of vanillate and verified by fluorescence microscopy and further verified by integration PCR.

JS761 NA1000 vanAmetK-YFP rnerne-CHYC Kan^R Gent^R. This strain was generated by transducing JS680 cells with pRNE-chy-4 phage lysate. The transduced cells were plated in PYE-Gent-Kan plates. The resulting colonies were grown in the presence and absence of vanillate and verified by fluorescence microscopy and further verified by integration PCR.

Article



JS735 NA1000 rnerne-msfGFP Gent^R. This strain was generated by transducing NA1000 cells with RNase E-msfGFP phage lysate from JS87⁴ strain. The transduced cells were plated in PYE-Gent plates. The resultant colonies were grown in PYE-Gent media and verified to be expressing the RNase E-msfGFP fusion by fluorescence microscopy.

JS744 NA1000 rnerne(Δhfg)-msfGFP Gent^R Spec^R Strp^R. This strain was generated by transducing Δhfg (Shapiro Lab, Stanford University School of Medicine) cells with RNase E-msfGFP phage lysate from JS87⁴ strain. The transduced cells were plated in PYE-Gent-Spec-Strp plates. The resultant colonies were grown in PYE-Gent-Spec-Strp and verified to be expressing the RNase E-msfGFP fusion by fluorescence microscopy.

JS671 NA1000 merne(∆rhIE)-msfGFP Gent^R Kan^R. This strain was generated by transducing RhIE disruption mutant (Marques Lab, University of Sao Paulo) cells with RNase E-msfGFP phage lysate from JS87⁴ strain. The transduced cells were plated in PYE-Gent-Kan plates. The resultant colonies were grown in PYE-Gent-Kan media verified to be expressing the RNase E-msfGFP fusion by fluorescence microscopy.

JS672 NA1000 rnerne(ΔrhlB)-msfGFP Gent^R. This strain was generated by transducing ΔrhlB (Marques Lab, University of Sao Paulo) cells with RNase E-msfGFP phage lysate from JS874 strain. The transduced cells were plated in PYE-Gent plates. The resultant colonies were grown in PYE-Gent media and verified to be expressing the RNase E-msfGFP fusion by fluorescence microscopy.

JS128 NA1000 popZ-Chy rne::pXrnessrAC Kan^R. This strain was generated by transducing cells harboring popZ-mCherry (native gene fusion) with RNase E depletion phage lysate from JS82 strain. The transduced cells were plated in PYE-Kan-Xylose plates and the resultant colonies were grown in PYE-Kan media with and without xylose to verify the RNase E depletion phenotype.

Strains used in bacterial two-hybrid assay

VNS003

The strain was created by transforming pVN054 and pVN057 plasmids into BTH101 cells and plated on LB-Agar plates containing Kanamycin, Ampicillin, IPTG and X-gal. The resultant colonies were selected based on blue or white color of the colonies.

VNS004

The strain was created by transforming pVN054 and pVN055 plasmids into BTH101 cells and plated on LB-Agar plates containing Kanamycin, Ampicillin, IPTG and X-gal. The resultant colonies were selected based on blue or white color of the colonies.

The strain was created by transforming pVN054 and pVN058 plasmids into BTH101 cells and plated on LB-Agar plates containing Kanamycin, Ampicillin, IPTG and X-gal. The resultant colonies were selected based on blue or white color of the colonies.

VNS006

The strain was created by transforming pKT25-Zip and pUT18C-Zip plasmids into BTH101 cells and plated on LB-Agar plates containing Kanamycin, Ampicillin, IPTG and X-gal. The resultant colonies were selected based on blue or white color of the colonies.

VNS007

The strain was created by transforming pKNT25 and pUT18 plasmids into BTH101 cells and plated on LB-Agar plates containing Kanamycin, Ampicillin, IPTG and X-gal. The resultant colonies were selected based on blue or white color of the colonies.

The strain was created by transforming pVN054 and pUT18 plasmids into BTH101 cells and plated on LB-Agar plates containing Kanamycin, Ampicillin, IPTG and X-gal. The resultant colonies were selected based on blue or white color of the colonies.

VNS009

The strain was created by transforming pKNT25 and pVN055 plasmids into BTH101 cells and plated on LB-Agar plates containing Kanamycin, Ampicillin, IPTG and X-gal. The resultant colonies were selected based on blue or white color of the colonies.

The strain was created by transforming pKNT25 and pVN058 plasmids into BTH101 cells and plated on LB-Agar plates containing Kanamycin, Ampicillin, IPTG and X-gal. The resultant colonies were selected based on blue or white color of the colonies.

BR-body enrichment assay and LC-MS proteomics

BR-body enrichment was performed as in.³⁰ Enriched BR-bodies were then resuspended in buffered SDS before proteomics sample

Suspension Trapping (S-Trap) Sample Preparation

100 μg protein lysate (JS221 or JS299) was prepared in triplicate according to the manufacturer's instructions. Trypsin was resuspended in a 50 mM ABC buffer and added to S-Traps at a 1:50 (enzyme:protein w/w) ratio and incubated for 8 h at 37°C. After the digestion, peptides were eluted according to the manufacturer's protocol and vacuum centrifuged to dryness prior to desalting.

Solid Phase Extraction (SPE)

All samples were desalted prior to MS analysis with 10mg HLB cartridges according to manufacturer's instructions as in. 73 Samples were dried prior to analysis and stored at -80° C until re-suspension for LC-MS.

Analysis via Nano UHPLC-MS/MS

Dried digests were resuspended in 0.1% formic acid in water to a concentration of 250 ng/µL. 2 µL of solution was injected onto a 100 mm × 100 μm C₁₈ BEH reverse phase chromatography column with an autosampler (nanoACQUITY, Waters Corporation).





Peptides were separated over a 95 min segmented gradient from 4 to 35% B (A = H₂O + 0.1% FA, B = acetonitrile +0.1% FA). MS-MS/MS was performed on a Q-Exactive HF mass spectrometer via electrospray ionization (Thermo Fisher Scientific). Samples were collected in biological triplicate, and data were acquired in technical triplicate injections using a TOP17 data-dependent method (DDA).

Peptide-Spectrum Matching (PSM)

RAW files from technical and biological triplicates were processed for peptide identification, protein inference, and false-discovery rate using the MetaMorpheus search engine. 45 A C. crescentus FASTA from UniProt (proteome ID UP000001364) was used with a common contaminant file. Data were first calibrated prior to search ('Traditional') using the default parameters. For 'Main' search, additional parameters included a maximum of two missed cleavages, two variable modifications per peptide, and a minimum peptide length of seven amino acids. The precursor mass tolerance was set to 5 ppm and the product mass tolerance was set to 20 ppm. The 'common' fixed and 'common' variable modifications were selected, and identifications were filtered to a q-value of <0.01. RAW data files are available through MassIVE with accession number (MSV000090894).

In vivo localization of BR-body associated proteins

All C. crescentus protein fusion strains were grown in PYE-Kan or PYE-Gent media overnight. The next day, from the mid-log phase cultures, serial dilutions were done in M2G medium containing the appropriate amount of Kan or Gent and cells were grown overnight. The next day, the mid-log phase cultures were induced with 0.5 mM vanillate and grown for 6 h. 1μL of the cells were spotted on a M2G 1.5% agarose pad, a coverslip was added, immersion oil was spotted on the coverslip, and the cells were imaged using a YFP filter cube.

RNase E depletion

Depletion strains containing the xylose-inducible copy of RNase E were first grown overnight in M2G-Kan-Gent medium containing 0.2% xylose. The next day, from the log-phase cultures, serial dilutions were prepared in M2G-Kan-Gent medium containing 0.2% xylose overnight. Mid-log phase cells were then washed 3 times with 1 mL growth medium, resuspended in growth medium, and split equally into two tubes. 0.2% xylose was added to one tube. Depletion strains were analyzed at the mid-exponential phase of growth (OD 0.3–0.6) and after 24 h of depletion of xylose. 1 μL of the cells under each condition were spotted on a M2G 1.5% agarose pad, a coverslip was added, immersion oil was spotted on the coverslip, and the cells were imaged using a YFP filter cube.

Colocalization of YFP tagged foci forming proteins with BR-body markers

Dual-labeled strains expressing foci-forming proteins in Figure 2A with BR-body markers RNase E or Aconitase were first grown in PYE medium containing the appropriate amount of Kan, Gent, Spec or Strp overnight. The next day, from log-phase cultures, serial dilutions were done in M2G medium. The following day, mid-log phase cells were split into two tubes, and one was treated with an inducer (0.5 mM vanillate or 0.02% xylose), and both were grown for 6 h. 1 μ L of the cells under each condition was spotted on a M2G 1.5% agarose pad, a coverslip was added, immersion oil was spotted on the coverslip, and the cells were imaged using YFP, CFP, GFP, and TX-Red filter cubes. A dual-labeled strain expressing PopZ-mCherry with RNase E-GFP was used as a negative control. Fluorescence level analysis of the droplets was performed using MicrobeJ. 40 Line traces were performed using ImageJ and the correlation analysis between channels was performed in Microsoft Excel.

In vivo localization of RNase E-GFP foci in the strains with BR-body enriched proteins deleted

JS671, JS672, JS735, and JS744 strains were grown in PYE medium containing the appropriate amount of Kan, Gent, Spec or Strp overnight. The next day, from the log-phase cultures, serial dilutions were done in M2G medium overnight. The following day, 1μL of the mid-log cells were spotted on a M2G 1.5% agarose pad, a coverslip was added, immersion oil was spotted on the coverslip, and the cells were imaged using a GFP filter cube.

Dissolution of MetK and ribosomal protein S1

Strains expressing MetK and ribosomal protein S1 with BR-body marker Aconitase-mCherry were first grown overnight in PYE-Kan-Spec-Strp medium in 3 serial dilutions. Mid-log phase cells were split equally into two tubes, one was treated with 0.2% xylose, and the cells were grown for 6 h. 1 μL of the cells under each condition was spotted on a M2G 1.5% agarose pad and imaged using TX-Red filter cubes.

Cell imaging

Around 1 µL of cells were immobilized on 1.5% agarose pads made with M2G medium on microscope slides (Thermo Fisher Scientific 3051). Cell droplets were allowed to air dry, were covered by a coverslip, and imaged with immersion oil. All images were collected using a Nikon Eclipse NI-E with CoolSNAP MYO-CCD camera and 100 x Oil CFI Plan Fluor (Nikon) objective, driven by Nikon elements software. The filter sets used for YFP, CFP, GFP, and mCherry imaging were chroma 96363, 96361, 96362, and 96322 models respectively. Cell image analysis was performed using MicrobeJ. 40

Article



RNA extraction

For RNA extraction, mid-log phase cells (0.3-0.5 OD600) were pelleted at 20,000 g for 10 min in a microcentrifuge. Then, the cells were resuspended in 1mL 65°C Trizol (1mL for each 1 mL of NA1000 cells) and incubated at 65°C for 10 min in a heat block. 200 µL of chloroform was added and incubated for 5 min at room temperature. The samples were then spun at max speed (20,000 g) in a microcentrifuge for 10 min at room temperature. The aqueous layer was removed and RNA samples were precipitated using 700 μL isopropanol at -80°C for 1 h and spun at 20,000 g for 1 h at 4°C. The supernatant was removed and the pellet was washed with 1 mL of 70% ethanol. The samples were then spun again for 10 min at 20,000 g at 4°C, the supernatant was removed, and the pellet was resuspended in RNase-free water. RNA samples were run on 1X TBE/7M urea denaturing PAGE gels and visualized with SYBR Gold nucleic acid gel stain.

Protein purifications

The protein coding genes were cloned into pET His6 MBP TEV, pET His6 G TEV, or pET28a plasmids and the expressed proteins were purified by His tag affinity purification, followed by the removal of the MBP or G tag by TEV proteolysis. RNase E CTD, RhIB, RhIE-IDR were expressed as N-terminal MBP fusions and all the other proteins were expressed as N-terminal G protein fusions. Briefly, the proteins were expressed in BL21 DE3 cells by inducing with 0.5mM IPTG at 37°C for 3.5 h in 2X Luria-Bertani medium. The cells were then pelleted at 5000 rpm for 20 min and were lysed in a lysis buffer (20mM Tris pH 7.4, 500mM NaCl, 10% glycerol, 10mM imidazole, 1mM PMSF, 1 tablet protease inhibitor cocktail, and DNase I) at 4°C using a sonicator with 10 s pulse on and 30 s pulse off times for 18 cycles. The lysed cells were centrifuged at 15,000 rpm for 45 min and the resultant supernatant was loaded onto equilibrated Ni-NTA resin, the protein-bound resin was washed with 10 column volumes each of lysis buffer, chaperone buffer (20 mM Tris pH 7.4, 1 M NaCl, 10% glycerol, 10 mM imidazole, 5 mM KCl, 10 mM MgCl2, and 2 mM ATP), and low salt buffer (20 mM Tris pH 7.4, 1 M NaCl, 10% glycerol, and 10 mM imidazole). The proteins were eluted in elution buffer (20 mM Tris pH 7.4, 150 mM NaCl, 10% glycerol, and 250 mM imidazole) and dialyzed into storage buffer (20 mM Tris pH 7.4, 150 mM NaCl). The contaminant proteins were removed by passing through an S200 size exclusion column. The concentrated proteins were stored at -80° C.

RNase E CTD purification: His6-MBP-TEV-RNase E CTD was expressed and purified in the same way as described above except the lysis buffer additionally contained 1M NaCl and 0.1% Triton X-100.

Hfg purification: Hfg protein was expressed at 18°C for 16 h. The lysis buffer and elution buffer contained 1 M NaCl instead of 150 mM and 500 mM NaCl, respectively. To remove the contaminating nucleic acids, the His tag affinity purified protein was treated with 30 µg/mL RNase A and 5 U/mL DNase I for 1 h at 37°C, concentrated, and loaded onto a HiLoad 16/60 Superdex 200 size exclusion column (GE healthcare). The absence of RNase A was further validated by incubating RNA with the protein.

Cyanine 5 protein labeling

Labeling reactions were carried out according to the manufacturer's protocol (Lumiprobe). Cy5 NHS ester dye dissolved in DMSO was incubated with proteins at an equal ratio in 0.1M sodium bicarbonate buffer pH 8.5 at room temperature for 4 h. A protein labeling calculator (https://www.lumiprobe.com/calc/protein-labeling) was used to calculate the amount of protein and dye used in the labeling reactions. The excess dye was removed by dialyzing against protein storage buffer (20mM Tris pH 7.4, 150mM NaCl) using a 3 kDa cut off dialysis cassette. Degree of labeling was calculated using the formula:

number of Cy5 dye per protein =
$$\frac{\text{molarity of Cy5 dye}}{\text{molarity of protein}}$$

[molarity of Cy5 dye] =
$$\frac{A650}{E650}$$

molarity of protein =
$$\frac{A2800}{E280}$$

A650 = conjugate absorbance at 650nm

£650 = molar extinction coefficient of Cy5 dye

A280c = conjugate corrected absorbance at <math>280nm = A280 - (A650 * (0.05))





£280 = molar extinction coefficient of protein

In vitro phase separation experiments and droplet assays

Proteins were incubated at their in vivo concentrations in the presence or absence of C. crescentus total RNA (20 ng/μL) in 20mM Tris pH 7.4, 100mM NaCl for 30 min at room temperature. The mixture was pipetted onto a glass slide, covered with a coverslip, and imaged using a Nikon epifluorescence microscope. For quantification of the number and distribution of droplets, 10 images for each protein were analyzed using the "analyze particles" function in ImageJ.

For the recruitment assays, 6 μM RNAse E CTD was incubated with 20 ng/μL of C. crescentus total RNA in 20mM Tris pH 7.4, 100mM NaCl for 20 min at room temperature, followed by the addition of Cy5-labeled client proteins and an additional incubation for 20 min before imaging. The level of recruitment was assessed by calculating the partition coefficient of client proteins. 30 droplets were analyzed in each case.

> mean fluorescence intensity inside the droplets partition coefficient = mean fluorescence intensity outside the droplets

ImageJ software was used to quantify the mean fluorescence and the data were plotted in PlotsOfData. 48 Co-assembly experiments were performed by mixing all the components and incubating for 30 min at room temperature before imaging.

For the salt and RNA dependency experiments, preformed protein and RNA condensates were incubated with either varying concentrations of NaCl or RNase A for 30 min at room temperature before the solution was imaged on a glass slide using phase contrast microscopy.

RNase E condensation induction in the absence of RNA was carried out by adding client proteins at varied concentrations to 6 µM RNase E CTD in 20mM Tris, 100mM NaCl and incubating for 30 min at room temperature. The solution was imaged on a glass slide using phase contrast microscopy.

In-vitro protein pull down assay

The RNAse E CTD tagged with maltose binding protein (MBP) or MBP only was incubated with prey proteins in pull down binding buffer (20mM HEPES pH 7.4, 100mM NaCl, 2% glycerol, and 2mM DTT) for 60 min at room temperature. 100 μL of dextrin agarose resin was added to the above mixture and incubated for another 90 min at 4°C on a tube rotator. The samples were washed four times with 1 mL of wash buffer (20mM HEPES pH 7.4, 100mM NaCl). Bound proteins were eluted with 100 μL of elution buffer (20mM HEPES pH 7.4, 150mM NaCl, 10mM maltose) at 30°C with constant shaking. The eluted proteins were resolved on an SDS PAGE gel.

Electrophoretic mobility shift assay

RNA (50 nM) was incubated with the specified concentrations of proteins for 30 min at room temperature in binding buffer (20mM Tris pH 7.4, 150mM NaCl, 5% glycerol, 2mM DTT, 1mM EDTA, and 10 μg/mL BSA). The incubated samples were resolved on a 5% acrylamide/bis-acrylamide native gel (prepared in TBE buffer) at 4°C in 0.5X TBE running buffer. The gel was stained with SYBR Gold for 20 min and scanned using a Typhoon scanner.

Bacterial two-hybrid assay

The bacterial two-hybrid assay was carried out as described previously in. 49 The bait protein RNase E was cloned into the pKNT25 plasmid (kanamycin resistance) using Xba1 and EcoR1 sites and the prey protein MetK was cloned into the pUT18 plasmid (ampicillin resistance) using Xba1 and Sac1 sites. The sequence verified plasmids were transformed into chemically competent BTH101 cells (adenylate cyclase deficient) and the colonies were selected on LB-agar plates containing kanamycin (50 μg/mL), ampicillin (100 μg/mL), X-gal (40 μg/mL), and IPTG (0.5mM), and incubated at 30°C for 72 h. The resultant blue colonies were grown in LB-medium containing kanamycin (30 μg/mL) and ampicillin (50 μg/mL) and log phase cells were plated onto LB-agar plates containing kanamycin, ampicillin, X-gal, and IPTG as mentioned above. The positive control cells were transformed with pKNT25-Zip and pUT18-Zip plasmids, which upon expression reconstitute a functional adenylate cyclase enzyme. The negative control cells were transformed with the pKNT25 and pUT18 plasmids.

Determination of the assembly order of RhIE, RNase E, and aconitase foci

C. crescentus JS716 (RhIE-YFP/Aconitase-mCherry) and JS452 (RNase E-YFP/Aconitase-mCherry) were grown overnight in PYE medium containing kanamycin (5 μg/mL), spectomycin (25 μg/mL), and streptomycin (5 μg/mL) until the cultures reached mid-log phase (OD ~0.3). Prior to imaging, the cells were diluted to 0.05 OD in PYE media and induced with 0.02% xylose for 15 min at 28°C. Aliquots of 1.5 μL of culture were spotted onto pads of 2% agarose in M2G medium and sandwiched between two coverslips. Cells were imaged with an Olympus IX71 inverted epifluorescence microscope with a 100 x objective (NA 1.40, oil immersion) kept at 28°C using an objective heater (Bioptechs). The YFP fusion proteins were imaged under excitation from a 488-nm laser (Coherent Cube 488-50; 0.4 W cm⁻²) and the mCherry fusions were imaged under excitation from a 561-nm laser (Coherent Sapphire

Cell Reports Article



561-50; 2.0 W cm⁻²). Both channels were imaged simultaneously on a 512 × 512 pixel Photometric Evolve electron-multiplying charge-coupled device (EMCCD) camera, using an OptoSplit II image splitter (Cairn Research) with a 635-nm long pass filter and a 525/50 nm bandpass filter. An integration time of 250 ms with a delay between frames of 5 s was used, where a shutter blocked irradiation during the delay time to minimize photobleaching of YFP and mCherry.

To analyze the fluorescence intensities, the mean intensity of each cell in each channel was first subtracted from the movies. Foci were then detected by eye in the background-subtracted movies, and the mean and maximum intensities within the 9 x 9 pixel region of interest (ROI) surrounding each focus was measured in both channels. Time zero was set to be the frame immediately preceding the first frame with an ROI mean intensity at least 10% higher than the maximum intensity value in the ROI in the previous frame. This time zero was also assigned as time zero on the other channel. Subsequently, the maximum intensity within the ROI was divided by the maximum intensity of the ROI in the time zero frame to determine the fluorescence intensity enhancement of each focus at each time.

Condensate growth kinetic assays

Time lapse images were acquired using a Zeiss LSM 800 microscope. 6 μM of RNase E CTD YFP (RCY) was spotted onto a glass slide, and either RNA or proteins or both at the specified concentrations were pipetted onto the RCY solution. Image acquisition was started before the addition of RNA or proteins or both, but the zero minute time point was calculated from the time they were added to the RCY solution on the glass slide. The zero minute time point for 'RCY only' started from the time the sample was spotted onto the glass slide. The images were acquired for 2.5 min with a 50 ms time interval. The data were quantified in ImageJ and plotted in MS Excel.

QUANTIFICATION AND STATISTICAL ANALYSIS

Foci quantification

In vivo protein fusion foci were quantified using MicrobeJ. 40 Cell outlines were first identified using the medial axis algorithm in the phase channel with a minimal cell length of 1.35 µm and the segmentation option. Cell outlines were then manually curated to remove cells containing erroneous outlines. Next, the maxima function was used with the "foci" option with a minimal area of 0.01 µm² and minimal length of 0.1 µm with the segmentation option on and the association inside option on. Tolerance and Z score parameters were tuned for each protein fusion type.

To quantify the average foci per cell of each strain, three replicates were performed on three different days and three images were analyzed from each day. We summed all foci identified in each cell and divided by the total number of cells to calculate number of foci per cell.

Colocalization analysis

Dual channel images of enriched BR-body protein fusions with BR-body markers were analyzed via the line trace method to assess colocalization. For each focus identified, we drew a line through the focus and quantified the intensity vector across the line. We then analyzed the other channel across the same line, and calculated the correlation of the intensity of each channel. The images were analyzed for a minimum of 30 foci identified in the BR-body enriched protein (presented in Figure 2B). PopZ-mCherry was used as a negative control for the analysis.

FRAP assays

FRAP was performed according to a standard protocol. ⁷⁴ Briefly, the measured F(t) over the bleached circular area of diameter (d) = 2 μm, normalized by that of the unbleached region of the same diameter, F(0), was fitted by a one-phase exponential function using the "Bottom to (Span+ Bottom)" analysis as $F(t)/F(0) = Bottom + Span^*(1 - exp(-t ln 2/\tau_{1/2}))$, where $\tau_{1/2}$ is the half-time for diffusion. The apparent diffusion coefficient, D, was obtained from $\tau_{1/2}$ according to D = d2/(4 $\tau_{1/2}$).